Inorganic Chemistry

Article

pubs.acs.org/IC

Interaction of Polycationic Ni(II)-Salophen Complexes with G-Quadruplex DNA

Laureline Lecarme,[†] Enora Prado,[†] Aurore De Rache,[‡] Marie-Laure Nicolau-Travers,[§] Romaric Bonnet,[†] Angeline van Der Heyden,[†] Christian Philouze,[†] Dennis Gomez,[§] Jean-Louis Mergny,[‡] Hélène Jamet,[†] Eric Defrancq,[†] Olivier Jarjayes,[†] and Fabrice Thomas*[,†]

[†]Université Grenoble Alpes, Département de Chimie Moléculaire, UMR CNRS 5250, BP 53, 38041 Grenoble Cedex 9, France

[‡]Inserm U869, Institut Européen de Chimie et Biologie IECB, Université de Bordeaux, 2 rue Robert Escarpit, 33607 Pessac, France

[§]CNRS, IPBS Institut de Pharmacologie et de Biologie Structurale, 205 Route de Narbonne, 31077 Toulouse Cedex 4, France

Supporting Information

ABSTRACT: A series of nine Ni(II) salophen complexes involving one, two, or three alkyl-imidazolium side-chains was prepared. The lengths of the side-chains were varied from one to three carbons. The crystal structure of one complex revealed a square planar geometry of the nickel ion. Fluorescence resonance energy transfer melting of G-quadruplex structures in the presence of salophen complex were performed. The G-quadruplex DNA structures were stabilized in the presence of the complexes, but a duplex DNA was not. The binding constants of the complexes for parallel and antiparallel G-quadruplex DNA, as well as hairpin DNA, were measured by surface plasmon resonance. The compounds were selective for G-quadruplex DNA, as reflected by equilibrium dissociation constant K_D values in the region 0.1−1 μM for G-quadruplexes and greater than 2 μM for duplex DNA. Complexes with more and shorter side-chains had the highest binding constants. The structural basis for the interaction of the complexes with the human telomeric G-quadruplex DNA was investigated by computational studies: the aromatic core of the complex stacked over the last tetrad of the G-quadruplex with peripherical cationic side chains inserted into opposite grooves. Biochemical studies (telomeric repeat amplification protocol assays) indicated that the complexes significantly inhibited telomerase activity with IC_{50} values as low as 700 nM; the complexes did not significantly inhibit polymerase activity.

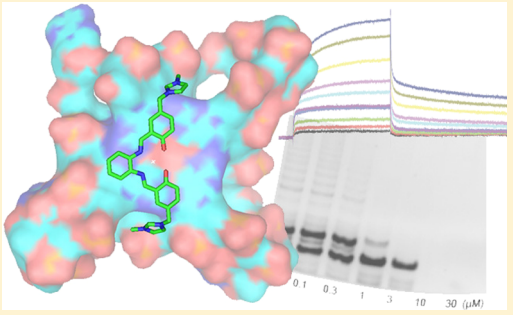

1. INTRODUCTION

Guanine-rich sequences are ubiquitous in genomes.[1] The presence of several consecutive guanines favors the folding of DNA into structures distinct from duplexes, known as G-quadruplexes.[2] G-quadruplexes consist of stacked planar arrangements of G-quartets, wherein four guanines interact through Hoogsteen hydrogen bonds.[3] An alkaline metal ion (such as potassium or sodium) is coordinated to the eight O6 carbonyl oxygens of two stacked guanine tetrads, stabilizing the G-quadruplex topology. G-quadruplexes are polymorphic due to the different possible arrangements of the strands (parallel, antiparallel, intra-, intermolecular).[4] Guanine-rich sequences are found at the extremities of eukaryotic chromosomes (i.e., the telomeric region)[5,6] and in promoter regions of certain oncogenes (c-myc) and in promoters of genes involved in the control of biologically important processes such as cell growth.[7]

Telomeres are typically 10−15 kilobases (kb) at birth for humans[8] and 20−50 kb for mice.[9] Telomeres are composed of double-stranded DNA with a 3′ overhanging, single-stranded region of 100−200 nucleotides.[10] The overhang consists of repeats of a short motif rich in guanines: G_3T_2A for humans,[11] G_4T_2 or G_4T_4 in the ciliates Tetrahymena[12] and Oxytricha,[13] respectively, and T_2AG_2 for insects and arthropods,[14] which fold into G-quadruplexes under certain conditions in vitro. The telomeres maintain genomic stability by protecting chromosome ends from the DNA repair machinery[15] and during the replication process.[16] DNA polymerases synthesize DNA only in one direction and require a primer, which is a short RNA or DNA strand. As a consequence, DNA replication is accompanied by the trimming of sequences from the ends of chromosomes. Once the chromosome attains a critical length the cell enters an irreversible growth arrest and does not replicate further (Hayflick's limit).[17] Telomere homeostasis is ensured by a protein complex called shelterin[18] and by the enzyme telomerase.[6,15,16] Telomerase adds copies of the repeat to the end of the telomere. This enzyme is transcriptionally repressed in normal somatic cells but overexpressed in approximately 85% of cancer cells.[19] This overexpression of telomerase thus prevents cellular senescence[20] and is believed to be a major step in the mechanisms that lead to immortalization of cancer cells.[21] Compounds that target telomeres are potential anticancer drugs:[22−27] their interaction

Received: August 25, 2014
Published: November 10, 2014

   dx.doi.org/10.1021/ic502063r | Inorg. Chem. 2014, 53, 12519−12531

Scheme 1. Representative G-Quadruplex Binders: (A) Telomestatin,[25a] (B) BRACO-19,[25b] (C) TMPyP4,[26c,f,h] and (D) Prototypical Nickel(II) Salophen Complex[27a]

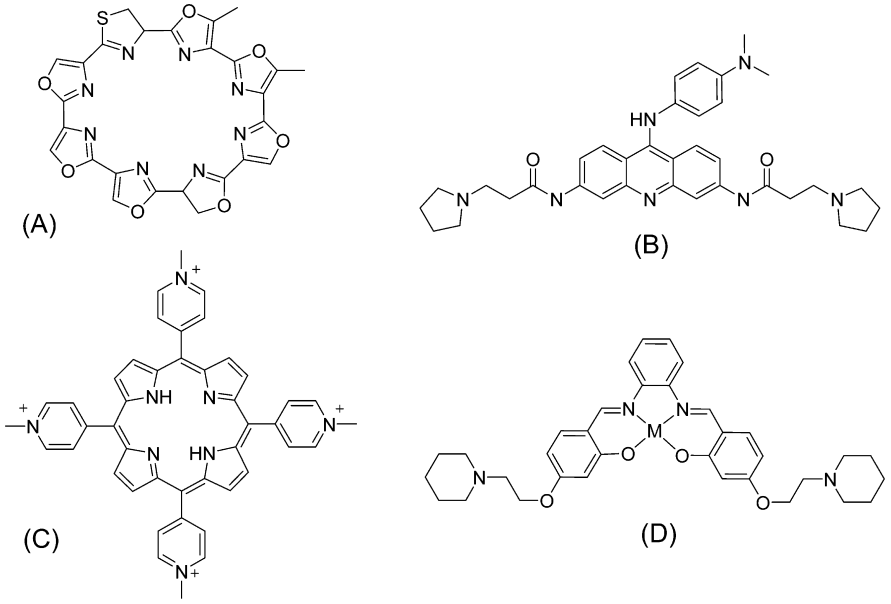

with G-quadruplexes should stabilize this structure,[25] inhibit the function of telomerase,[28] and confer mortality to cancer cells.[29,30]

During the past few years a number of G-quadruplex binders have been synthesized and characterized (Scheme 1),[22−27] providing insight into the structural requirements for efficient molecular recognition of the G-quadruplex structure.[23,24] The most potent G-quadruplex binders contain aromatic rings that interact through $\pi-\pi$ stacking with a G-quartet. Inorganic complexes[24,26,27] are particularly interesting because metal coordination is expected to decrease the π electron density on the aromatic ligand, thereby increasing their potential to stack on the tetrad.[27d] The metal ion may also interact with the carbonyl groups of the tetrads that define the central ion-binding channel to optimally position the complex.[24] The most efficient G-quadruplex binders also contain additional cationic groups that may be involved in electrostatic interactions with the phosphates located in the grooves. Two families of inorganic G-quadruplexes binders are the porphyrins[26] and the salophen complexes[27] (Scheme 1). Pioneering works by Neidle and colleagues revealed that salophens bind strongly to the human telomeric G-quadruplexes and inhibit telomerase activity with EC_{50} of roughly 0.1 μM.[27a] A binding mode was initially proposed on the basis of docking studies,[27a] and a crystal structure of a salophen−quadruplex adduct is available.[27d] The crystal structure revealed that the complex is positioned on a terminal tetrad with the metal ion located over the potassium channel and with each aromatic ring involved in $\pi-\pi$ interactions with guanines. The two morpholinium side-chains are inserted into adjacent grooves with each interacting with a phosphate group.[27d]

The nature of the metal ion in the salophen complex influences binding affinity for G-quadruplex; nickel(II) is optimal.[27b] The length of the side-chains, their positions on the salophen scaffold, and the type of cationic group also impact binding affinity, but the roles of these functional groups are not well understood.

In this article we report on the synthesis of a new family of G-quadruplex binders that is based on the nickel(II) salophen platform (Scheme 2). The side-chains are alkyl-imidazolium arms connected para to the phenol moieties. With alkyl-imidazolium arms pointing in opposite directions we envisioned that the side-chains would favorably interact with opposite grooves of DNA G-quadruplexes. We also evaluated functionalization on the diaminobenzene ring with an alkylimidazolium chain. The affinity for G-quadruplex and duplex DNA was assessed by different methods including surface plasmon resonance (SPR) studies and fluorescence resonance energy transfer (FRET)-based melting experiments. In addition, the binding mode was studied by computational methods. Finally, the inhibition of telomerase was evaluated using telomeric repeat amplification protocol (TRAP) assays.

Scheme 2. Structures of Complexes 1−9

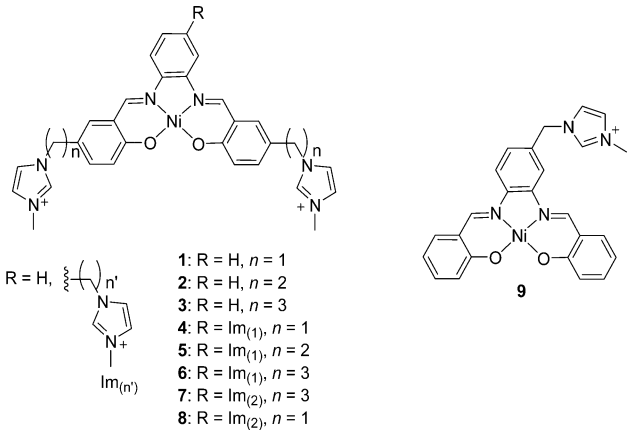

2. EXPERIMENTAL SECTION

2.1. Materials and Instruments. NMR spectra were recorded on a Bruker AM 300 (^{1}H at 300 MHz, ^{13}C at 75 MHz) or a Bruker Avance 400 (^{1}H at 400 MHz, ^{13}C at 100 MHz) spectrometer. Chemical shifts are given relative to the residual solvent peak. Mass spectra were recorded on a Bruker Esquire 3000 (ESI/Ion Trap) equipment. Microanalysis was performed by the Service Central

dx.doi.org/10.1021/ic502063r | Inorg. Chem. 2014, 53, 12519−12531

d'Analyse du CNRS (Lyon, France). UV−visible−near-infrared spectra were recorded on a Cary Varian 50 spectrophotometer. The quartz cell path length was 1 cm.

2.2. Crystal Structure Analysis. Collected reflections were corrected for Lorentz and polarization effects by using SADABS-2004/1. The structure was solved by direct methods and refined using the OLEX2 software.[31] All non-hydrogen atoms were refined with anisotropic thermal parameters. Hydrogen atoms were generated in idealized positions on the carrier atoms with isotropic thermal parameters; the exceptions were the hydroxyl groups, which were localized on the Fourier map and fixed. Additional crystallogaphic data are available in the Supporting Information.

2.3. Computational Details. An initial docking was performed for **4**. The complex geometry was optimized at B3LYP/6-31g using the Gaussian09 software.[32] The Autodock 3.0 package[33] was used for the docking calculations on the crystal structure of parallel G-quadruplexes for human telomeric DNA (PDB code:1KF1).[3c] A grid box of 90 × 90 × 90 points with a spacing of 0.375 Å between the grid points was used. The single bonds of the side chain were treated as active torsional bonds. The Ni parameters were set as r = 1.170 Å, q = +2.0, and van der Waals well depth was 0.100 kcal/mol. One hundred docked structures (i.e., 100 runs) were generated by using genetic algorithm searches. A default protocol was applied with an initial population of 50 randomly placed individuals, a maximum number of 2.5×10^5 energy evaluations, a maximum number of 2.7×10^4 generations, a mutation rate of 0.02, and a crossover rate of 0.8. Docking input files for the complex and the G-quadruplex were generated with the Sybyl 7.3 software.[34] For the docking calculations on the G-quadruplex, only polar hydrogen atoms were added, and the Kollman unified partial charges were assigned. For the complex, Gasteiger-Huckel partial charges were chosen. Results differing by less than 1 Å in positional root-mean-square-deviation (RMSD) were clustered together and represented by the result with the most favorable free energy of binding. Then the docked position was used as a template to construct the systems formed by the different complexes and the first layer of the G-quadruplex. All the hydrogen atoms were now added on the G-quadruplex. This was accomplished with the Gaussview interface. Then using Gaussian09, all the parts of the G-quadruplex were frozen, and positions of the complexes were optimized at PM6 level. NCI computations were then performed using the NCI-Plotpackage[35] with the promolecular densities. Single energy calculations at ωB97XD/6-311++(2d,p)(C,H,O,N)/lanl2dz (Ni, P) level were done to evaluate the strengths of various interactions.

2.4. FRET Melting. FRET melting experiments were carried out in 96-well plates on a real-time polymerase chain reaction (PCR) equipment (Stratagene Mx3005P) as previously described.[36] The excitation and detection wavelengths were 492 and 516 nm, respectively. After a 5 min stabilization at 25 °C, the temperature was increased by 1 °C every minute until 95 °C. Each experimental condition was tested in duplicate on at least three separate plates. The oligonucleotides used for the determination of the ligand-induced thermal stabilization ($\Delta T_{1/2}$) are listed in Table S1 in the Supporting Information. They were purchased from Eurogentec, dissolved in pure water to an approximate 0.5 mM stock concentration, and stored at −20 °C. The exact stock concentrations were determined from the absorbance at 260 nm (measured on a Uvikon XS spectrophotometer) using molar extinction coefficients given on technical data sheets. The melting experiments were performed at a final 0.2 μM strand concentration of oligonucleotide with 0.5 μM of ligand (stock concentration: 10 mM in DMSO). The measurement buffer contained 10 mM lithium cacodylate (pH 7.2) and either 10 mM KCl and 90 mM LiCl (for DNA sequences) or 1 mM KCl and 99 mM LiCl (for RNA sequences). Before the ligand addition, the oligonucleotides were heated at 90 °C for 2 min and subsequently ice-cooled to favor their intramolecular folding and the initial FAM quenching.

2.5. Surface Plasmon Resonance Studies. SPR measurements were performed on a BIAcore T100 (GE Healthcare) operating with the BIAcoreT100 evaluation control Software 2.0.1. All measurements were performed at 25 °C in 0.01 M *N*-(2-hydroxyethyl)piperazine-*N*′-ethanesulfonic acid (HEPES) (pH 7.4), 0.15 M NaCl, 0.2 M KCl, and 0.05% (v/v) surfactant P20. The biomolecular systems containing the G-quadruplexes and the duplex were prepared as previously reported.[37] Briefly, this system is composed of (i) an intermolecular-like G-quadruplex **A**, $d[TTAGGGT]_4$; (ii) an intramolecular-like G-quadruplex **B** formed by the sequence $d(GGG(TTAGGG)_3TT)$; or (iii) a hairpin duplex **C**, d(CGCGCGCGTTTTCGCGCGCG). The different oligonucleotides were immobilized on streptavidin-coated surfaces (SA sensor chip, Biacore) to obtain a response of ∼500 RU. A nonmodified channel was used as reference. Binding experiments were conducted at 30 μL min^{-1} by injection of the ligand (300 s of association time) on the four channels. Regeneration of the surface was achieved by injection of a 1 M NaCl, 0.05% SDS aqueous solution for complexes **4**−**7** and by injection of a 1 M NaCl aqueous solution for complex **8**. No regeneration step was required for complexes **1**−**3**. Curves obtained on the reference surface were subtracted from the curves recorded on the other ones, allowing elimination of refractive index changes due to buffer effects and correction of nonspecific interactions. The rate constants for binding of the complexes to DNA were calculated by a nonlinear regression of the association and dissociation curves using the BIAcore T100 evaluation tool (release 2.0.1). The data were fitted using a heterogeneous ligand model. From the analysis of the sensorgrams, the association rate constants, k_{on1} and k_{on2}, and the dissociation rate constants, k_{off1} and k_{off2}, as well as the theoretical maximal responses, R_{max1} and R_{max2}, for the two interactions were calculated. Finally, the equilibrium dissociation constants were calculated from the binding rate constants as $K_{D1} = k_{off1}/k_{on1}$ and $K_{D2} = k_{off2}/k_{on2}$. The data presented in the manuscript are related to the interaction leading to the maximum theoretical response R_{max}.

2.6. TRAP-G_4 Assay. Telomerase active extracts were prepared from HT1080 cells overexpressing hTERT protein.[38] Inhibition of telomerase activity by small molecules was assessed using the modified telomere repeat amplification, TRAP-G_4, described in ref 39. Briefly, PCR was performed in a final 25 μL reaction volume composed of 20 mM Tris-HCl (pH 8.0), 50 μM deoxynucleotide triphosphates, 1.5 mM $MgCl_2$, 63 mM KCl, 1 mM EGTA, 0.005% Tween 20, 20 μg mL^{-1} BSA, 70 nM of TSG_4 (5′-GGGATTGGGATTGGGATTGGGTT-3′), 360 nM of TS (5′-AATCCGTCGAGCAGAGTT-3′), 450 nM of CXext (5′-GTGCCCTTACCCTTACCCTTACCCTAA-3′), 150 nM of NT (5′-ATCGCTTCTCGGCCTTTT-3′), 200 nM TSNT, internal control (ITAS) (5′-ATTCCGTCGAGCAGAGTTAAAAGGCCGAGAAGCGAT-3′), 2.5 units of Taq DNA polymerase, and 100 ng of telomerase. After amplification, 5 μL of loading buffer containing 20% sucrose, 0.2% bromphenol blue, and 0.2% xylene cyanol in Tris-borate-ethylenediaminetetraacetic acid buffer were added to the reaction. A 10 μL aliquot was loaded onto a 12% nondenaturing acrylamide gel (19:1) in TBE 1X band electrophoresed at 180 V for 1 h. Gels were stained with SYBR Green I (molecular probes) and digitalized by a photoimager (Bio-Rad).

2.7. Syntheses. *Compound* ***Ib.*** Compound **Ib** was prepared according to a slight modification of a synthesis described[40] using hexamethylenetetramine (HMTA) instead of Grignard reagent, paraformaldehyde, and triethylamine.

3-(3-Formyl-4-hydroxyphenethyl)-1-methyl-1H-imidazol-3-ium ***(Ic).*** Compound **Ib** (1 g, 2.8 mmol) was dissolved in toluene (12 mL), and *N*-methylimidazole (245 mg, 2.8 mmol) was added. The reaction mixture was stirred at room temperature (r.t.) for 6 h until the formation of a yellow precipitate, which was collected by filtration and washed with a minimum of cold toluene. A pure yellow solid was obtained. Yield: 70%. Mp = 139.9−141.3 °C. ^{1}H NMR (400 MHz, [D_6]dimethyl sulfoxide (DMSO)): δ = 10.95 (s, 1H, CHO); 10.46 (s, 1H, Ph−OH); 9.93 (s, 1H, N═CH-N); 7.67 (d, J = 2.2 Hz, 1H, imid-H); 7.40 (dd, J = 2.2 Hz, J = 8.5 Hz, 1H, imid-H); 7.08 (d, J = 8.5 Hz, 2H, Ar−H); 6.92 (d, J = 8.5 Hz, 1H, Ar−H); 4.66 (t, J = 7.2 Hz, 2H, $-CH_2$); 4.02 (s, 3H, $N-CH_3$); 3.30 (t, J = 7.2 Hz, 2H, $-CH_2$) ppm; ^{13}C NMR (100 MHz, [D_6]DMSO): δ = 191.5, 160.1, 137.2, 136.9, 129.2, 128.2, 124.0, 122.8, 122.7, 118.0, 50.2, 36.3, 34.8 ppm. ESI MS: m/z = 231.1 $[M\text{-}I^-]^+$. Anal. Calcd for $C_{13}H_{15}IN_2O_2$ (358.17): C 43.60, H 4.23, N 7.83. Found: C 43.48, H 4.39, N 7.99%.

dx.doi.org/10.1021/ic502063r | *Inorg. Chem.* 2014, 53, 12519−12531

*2-Hydroxy-5-(3-iodopropyl)benzaldehyde (**IIb**).* Product **IIa** (800 mg, 3.05 mmol) was mixed with hexamethylenetetramine (435 mg, 3.1 mmol) in trifluoroacetic acid (TFA) (6 mL) and refluxed for 2 h. After cooling, the reaction mixture was poured into 4 M HCl (20 mL) and stirred for 1 h, after which it was extracted with CH_2Cl_2 (2 × 20 mL). The combined organic extracts were washed with 4 M HCl (2 × 20 mL) and then in saturated brine (20 mL), and then they were dried (Na_2SO_4) and evaporated to give an orange oil. The product was purified by chromatography (silica gel, CH_2Cl_2) giving product **IIb** as orange oil. Yield: 56%. ^{1}H NMR (400 MHz, $CDCl_3$): δ = 10.88 (s, 1H, CHO); 9.88 (s, 1H, Ph−OH); 7.38 (m, 2H, Ar−H); 6.94 (d, J = 7.2 Hz, 1H, Ar−H); 3.17 (t, J = 7 Hz, 2H, $-CH_2$); 2.74 (t, J = 7 Hz, 2H, $-CH_2$); 2.13−2.09 (m, 2H, $-CH_2$) ppm; ^{13}C NMR (100 MHz, $CDCl_3$): δ = 196.5, 160.2, 137.4, 133.1, 131.8, 120.5, 117.8, 34.9, 34.6, 5.7 ppm. Electrospray ionization mass spectrometry (ESI MS): m/z = 288.8 $[M\text{-}H^+]^-$. Anal. Calcd for $C_{10}H_{11}IO_2$ (290.10): C 41.41, H 3.83. Found: C 40.89, H 3.97%.

*3-(3-(3-Formyl-4-hydroxyphenyl)propyl)-1-methyl-1H-imidazol-3-ium iodide (**IIc**).* Compound **IIb** (500 mg, 1.7 mmol) and *N*-methylimidazole (140 mg, 1.7 mmol) were dissolved in toluene (6 mL). After refluxing for 2 d, the cooled precipitate was filtrated to give a pure gray solid. Yield: 90%. Mp = 183.6−242.4 °C. ^{1}H NMR (400 MHz, [D_6]DMSO): δ = 10.56 (s, 1H, CHO); 10.25 (s, 1H, Ph−OH); 9.10 (s, 1H, N═CH-N); 7.77 (t, J = 1.65 Hz, 1H, Ar−H); 7.69 (d, J = 1.65 Hz, 1H, Ar−H); 7.47 (d, J = 2.4 Hz, 1H, imid-H); 7.37 (dd, J = 2.4 Hz, J = 8.4 Hz, 1H, imid-H); 6.93 (d, J = 8.4 Hz, 1H, Ar−H); 4.17 (t, J = 7.2 Hz, 2H, $-CH_2$); 3.83 (s, 3H, N−CH_3); 2.56 (t, J = 7.2 Hz, 2H, $-CH_2$); 2.12−2.02 (m, 2H, $-CH_2$) ppm; ^{13}C NMR (100 MHz, [D_6]DMSO): δ = 192.0, 159.6, 137.1, 137.0, 131.9, 128.7, 124.1, 122.7, 122.5, 117.8, 48.9, 36.3, 31.2, 31.0 ppm. ESI MS: m/z = 245.1 $[M\text{-}I^-]^+$. Anal. Calcd for $C_{14}H_{17}IN_2O_2$ (372.20): C 45.18, H 4.61, N 7.53. Found: C 45.34, H 4.84, N 7.78%.

*4-(Bromomethyl)-1,2-dinitrobenzene (**IIIa**).* This product was prepared by refluxing a mixture of (3,4-dinitrophenyl)methanol (1 g, 5 mmol) and 48% hydrobromic acid (30 mL) for 6 h. After the mixture was cooled, it was poured into water (30 mL) and stirred for 30 min, after which it was extracted with diethyl ether (2 × 30 mL). The combined organic extracts were washed with water (30 mL) and then saturated $NaHCO_3$ (30 mL), and then they were dried (Na_2SO_4) and evaporated to give a dark-yellow oil sufficiently pure for the next reaction. Yield: 90%. ^{1}H NMR (400 MHz, $CDCl_3$): δ = 7.92 (d, J = 8.1 Hz, 2H, Ar−H); 7.76 (d, J = 8.1 Hz, 1H, Ar−H); 4.52 (s, 2H, $-CH_2$) ppm; ^{13}C NMR (100 MHz, $CDCl_3$): δ = 144.5, 143.2, 142.1, 133.5, 125.7, 125.5, 29.1 ppm. ESI MS: m/z = 258.9 $[M\text{-}H^+]^-$. Anal. Calcd for $C_7H_5BrN_2O_4$ (261.03): C 32.21, H 1.94, N 10.74. Found: C 32.83, H 1.57, N 10.74%.

*3-(3,4-Dinitrobenzyl)-1-methyl-1H-imidazol-3-ium bromide (**IIIb**).* This preparation closely followed the synthesis of **Ic**, starting from **IIIa** (1.17 g, 4.5 mmol) and *N*-methylimidazole (370 mg, 4.5 mmol) in acetone (40 mL). After a 3 h reflux, the precipitate was filtrated to give a yellow powder. Yield: 80%. Mp = 226.3−226.4 °C. ^{1}H NMR (400 MHz, [D_6]DMSO): δ = 9.19 (s, 1H, N═CH-N); 8.32−8.30 (m, 2H, Ar−H); 7.97 (dd, J = 1.7 Hz, J = 8.2 Hz, 1H, Ar−H); 7.80 (t, J = 1.7 Hz, 1H, imid-H); 7.74 (t, J = 1.7 Hz, 1H, imid-H); 5.63 (s, 2H, $-CH_2$); 3.86 (s, 3H, N−CH_3) ppm; ^{13}C NMR (100 MHz, [D_6]DMSO): δ = 142.5, 142.3, 142.2, 137.8, 134.5, 126.7, 126.0, 124.6, 122.8, 50.5, 36.5 ppm. ESI MS: m/z = 263.0 $[M\text{-}Br^-]^+$. Anal. Calcd for $C_{11}H_{11}BrN_4O_4$ (343.13): C 38.51, H 3.24, N 16.33. Found: C 39.22, H 3.23, N 16.76%.

*3-(3,4-Diaminobenzyl)-1-methyl-1H-imidazol-3-ium bromide (**IIIc**).* Compound **IIIb** (1.2 mg, 3.5 mmol) was dissolved in methanol (50 mL), and 10% Pd/C (50% water, 825 mg) was added. The reaction mixture was stirred under 20 bar H_2 for 2 h. The reaction mixture was filtered through Celite and washed with methanol. Then the filtrate was evaporated to give a brown solid. Yield: 96%. Mp = 238.6−238.7 °C. ^{1}H NMR (400 MHz, [D_6]DMSO): δ = 9.07 (s, 1H, N═CH-N); 7.65 (s, 2H, imid-H); 6.49−6.46 (m, 3H, Ar−H); 5.09 (s, 2H, $-CH_2$); 4.62 (s, 2H, -NH_2); 4.55 (s, 2H, -NH_2); 3.82 (s, 3H, N−CH_3) ppm; ^{13}C NMR (100 MHz, [D_6]DMSO): δ = 136.5, 136.1, 135.6, 124.1, 123.1, 122.6, 118.3, 114.8, 114.7, 53.0, 36.2 ppm. ESI MS: m/z = 203.1 $[M\text{-}Br^-]^+$. Anal. Calcd for $C_{11}H_{15}BrN_4.H_2O$ (301.18): C 43.87, H 5.69, N 18.60. Found: C 43.56, H 5.23, N 18.22%.

*4-Acetamido-3-nitrophenethyl acetate (**IVb**).* Compound **IVa** (1 g, 4.5 mmol) was mixed with acetic anhydride (850 μL, 9 mmol) in CH_2Cl_2. The solution was cooled at 0 °C in a water/ice bath, and fuming nitric acid (440 μL) was added dropwise. After 1 h of stirring at 0 °C, the mixture was poured into water (20 mL) and stirred for 30 min, after which it was extracted with CH_2Cl_2 (2 × 20 mL). The combined organic extracts were washed with water (20 mL), then dried (Na_2SO_4) and evaporated to give a pure orange solid. Yield: 98%. Mp = 108.9−119.4 °C. ^{1}H NMR (400 MHz, $CDCl_3$): δ = 10.22 (s, 1H, -NH); 8.68 (d, J = 8.7 Hz, 1H, Ar−H); 8.05 (d, J = 2 Hz, 1H, Ar−H); 7.49 (dd, J = 2 Hz, J = 8.7 Hz, 1H, Ar−H); 4.27 (t, J = 6.6 Hz, 2H, $-CH_2$); 2.95 (t, J = 6.6 Hz, 2H, $-CH_2$); 2.27 (s, 3H, $-CH_3$); 2.02 (s, 3H, $-CH_3$) ppm; ^{13}C NMR (100 MHz, $CDCl_3$): δ = 170.8, 169.0, 136.5, 136.3, 133.6, 133.4, 125.6, 122.4, 63.9, 34.0, 25.5, 20.8 ppm. ESI MS: m/z = 267.1 $[M+H^+]^+$. Anal. Calcd for $C_{12}H_{14}N_2O_5$ (266.25): C 54.14, H 5.30, N 10.53. Found: C 54.04, H 5.24, N 11.00%.

*2-(4-Amino-3-nitrophenyl)ethanol (**IVc**).* Compound **IVb** (800 mg, 3 mmol) was dissolved in methanol (7 mL), and 10 M NaOH was added (300 μL, 3 mmol). The mixture was stirred for 15 min and evaporated under vacuum to give a brown oil used directly without further purification. Yield: 78%. ^{1}H NMR (400 MHz, [D_6]DMSO): δ = 7.77 (d, J = 2 Hz, 1H, Ar−H); 7.32 (s, 2H, -NH_2); 7.27 (dd, J = 2 Hz, J = 8.6 Hz, 1H, Ar−H); 6.94 (d, J = 8.6 Hz, 1H, Ar−H); 3.54 (t, J = 6.7 Hz, 2H, $-CH_2$); 2.60 (t, J = 6.7 Hz, 2H, $-CH_2$) ppm; ^{13}C NMR (100 MHz, [D_6]DMSO): δ = 153.7, 134.9, 127.8, 125.8, 124.6, 123.8, 62.1, 38.4 ppm. ESI MS: m/z = 181.0 $[M\text{-}H^+]^-$. Anal. Calcd for $C_8H_{10}N_2O_3.1.5NaOH.H_2O$ (260.19): C 36.93, H 5.23, N 10.77. Found: C 37.01, H 5.16, N 9.72%.

*4-(2-Bromoethyl)-2-nitroaniline (**IVd**).* **IVc** (455 mg, 2.5 mmol) was mixed with 48% hydrobromic acid (15 mL) and refluxed for 6 h. After it cooled at r.t., the mixture was poured into water (20 mL) and stirred for 30 min, after which it was extracted with diethyl ether (2 × 20 mL). The combined organic extracts were washed with water (20 mL) and then saturated $NaHCO_3$ (20 mL), and then they were dried (Na_2SO_4) and evaporated to give an orange oil. Yield: 52%. %. ^{1}H NMR (400 MHz, $CDCl_3$): δ = 7.97 (d, J = 2 Hz, 1H, Ar−H); 7.23 (dd, J = 2 Hz, J = 8.5 Hz, 1H, Ar−H); 6.77 (d, J = 8.5 Hz, 1H, Ar−H); 3.53 (t, J = 7.2 Hz, 2H, $-CH_2$); 3.08 (t, J = 7.2 Hz, 2H, $-CH_2$) ppm; ^{13}C NMR (100 MHz, $CDCl_3$): δ = 143.6, 136.4, 130.4, 127.7, 125.7, 119.1, 37.7, 32.7 ppm. ESI MS: m/z = 165.1 $[M\text{-}Br^-]^+$. Anal. Calcd for $C_8H_9BrN_2O_2.0.25C_4H_{10}O$ (263.60): C 41.01, H 4.40, N 10.63. Found: C 40.80, H 4.08, N 10.70%.

*3-(4-Amino-3-nitrophenethyl)-1-methyl-1H-imidazol-3-ium bromide (**IVe**).* This preparation closely followed the synthesis of **Ic**, starting from **IVd** (400 mg, 1.6 mmol) and *N*-methylimidazole (130 mg, 1.6 mmol) in acetone (15 mL). After a 2 d reflux, the precipitate was filtered to give an orange powder. Yield: 78%. Mp = 189.8−196.3 °C. ^{1}H NMR (400 MHz, [D_6]DMSO): δ = 9.04 (s, 1H, N═CH-N); 7.78 (d, J = 2 Hz, 1H, Ar−H); 7.72 (t, J = 1.7 Hz, 1H, imid-H); 7.67 (t, J = 1.7 Hz, 1H, imid-H); 7.36 (s, 2H, -NH_2); 7.25 (dd, J = 2 Hz, J = 8.7 Hz, 1H, Ar−H); 6.96 (d, J = 8.7 Hz, 1H, Ar−H); 4.37 (t, J = 7.2 Hz, 2H, $-CH_2$); 3.81 (s, 3H, N−CH_3); 3.02 (t, J = 7.2 Hz, 2H, $-CH_2$) ppm; ^{13}C NMR (100 MHz, [D_6]DMSO): δ = 145.2, 136.5, 136.4, 129.9, 124.9, 123.9, 123.5, 122.3, 119.6, 49.6, 35.7, 34.0 ppm. ESI MS: m/z = 247.1 $[M\text{-}Br^-]^+$. Anal. Calcd for $C_{12}H_{15}BrN_4O_2.1/2H_2O$ (336.18): C 42.87, H 4.80, N 16.67. Found: C 43.09, H 4.71, N 16.31%.

*3-(3,4-Diaminophenethyl)-1-methyl-1H-imidazol-3-ium bromide (**IVf**).* Compound **IVe** (306 mg, 1 mmol) was dissolved in methanol (15 mL), and 10% Pd/C (50% water, 110 mg) was added. The reaction mixture was stirred under H_2 (20 bar) for 2 d. The mixture was filtered through Celite, washed with methanol, and the extracts were evaporated to give a brown solid. Yield: 81%. Mp = 234.2−234.3 °C. ^{1}H NMR (400 MHz, [D_6]DMSO): δ = 9.01 (s, 1H, N═CH-N); 7.69 (d, J = 1.7 Hz, 1H, Ar−H); 7.66 (t, J = 1.7 Hz, 1H, imid-H); 6.42 (d, J = 7.8 Hz, 1H, imid-H); 6.31 (d, J = 7.8 Hz, 1H, -NH_2); 6.18 (dd, J = 1.9 Hz, J = 7.8 Hz, 1H, Ar−H); 4.41 (s, 4H, -NH_2); 4.28 (t, J = 7.3

dx.doi.org/10.1021/ic502063r | *Inorg. Chem.* 2014, 53, 12519−12531

Hz, 2H, $-CH_2$); 3.82 (s, 3H, N$-CH_3$); 2.85 (t, J = 7.3 Hz, 2H, $-CH_2$) ppm; ^{13}C NMR (100 MHz, [D_6]DMSO): δ = 136.9, 135.6, 134.2, 125.5, 123.9, 122.8, 117.6, 115.1, 115.0, 50.8, 36.2, 35.6 ppm. ESI MS: m/z = 217.1 [M-Br$^-$]$^+$. Anal. Calcd for $C_{12}H_{17}BrN_4.H_2O$ (315.21): C 45.72, H 6.08, N 17.77. Found: C 45.66, H 5.47, N 17.33%.

Complex **1**. To a solution of 3-(3-formyl-4-hydroxybenzyl)-1-methyl-1*H*-imidazol-3-ium[41] chloride (100 mg, 0.4 mmol) dissolved in MeOH (4 mL) was added $Ni(OAc)_2{\cdot}4H_2O$ (50 mg, 0.2 mmol) in MeOH (2 mL) and *o*-phenylenediamine (21.5 mg, 0.2 mmol) in MeOH (2 mL). Triethylamine (60 μL, 0.43 mmol) was added to the resulting red solution. The reaction mixture was refluxed for 1 d. After it cooled at r.t., the mixture was evaporated and taken up in diethyl ether. The precipitate was then filtered to give a red hygroscopic powder. Yield: 47%. ^{1}H NMR (400 MHz, [D_6]DMSO): δ = 9.34 (s, 2H, -N=CH); 9.15 (s, 2H, -N=CH-N); 8.18−8.16 (m, 2H, Ar−H); 7.78 (d, J = 9.5 Hz, 4H, imid-H); 7.73 (s, 2H, Ar−H); 7.40−7.34 (m, 4H, Ar−H); 6.90 (d, J = 8.8 Hz, 2H, Ar−H); 5.35 (s, 4H, $-CH_2$); 3.88 (s, 6H, N$-CH_3$) ppm; ESI MS: m/z = 281.1 [M-2Cl$^-$]$^{2+}$. Anal. Calcd for $C_{30}H_{28}Cl_2N_6NiO_2.8H_2O$ (778.30): C 46.30, H 5.70, N 10.80. Found: C 46.60, H 5.93, N 10.52%. λ (nm)/ε ($M^{-1}{\cdot}cm^{-1}$), HEPES-buffered saline (pH 7.4): 365 (20500).

Complex **2**. This preparation closely followed the synthesis of complex **1**, starting from **Ic** (100 mg, 0.28 mmol) in MeOH (4 mL), $Ni(OAc)_2{\cdot}4H_2O$ (35 mg, 0.14 mmol) in MeOH (2 mL), *o*-phenylenediamine (15 mg, 0.14 mmol) in MeOH (2 mL), and triethylamine (43 μL, 0.31 mmol) were added. A red hygroscopic solid was obtained. Yield: 42%. ^{1}H NMR (400 MHz, [D_6]DMSO): δ = 9.01 (s, 2H, -N=CH); 8.80 (s, 2H, -N=CH-N); 8.10−8.11 (m, 2H, Ar−H); 7.71 (s, 2H, imid-H); 7.67 (s, 2H, imid-H); 7.35 (s, 4H, Ar−H); 7.18 (d, J = 8.4 Hz, 2H, Ar−H); 6.84 (d, J = 8.4 Hz, 2H, Ar−H); 4.40−4.36 (m, 4H, $-CH_2$); 3.82 (s, 6H, N$-CH_3$); 3.05−3.01 (m, 4H, $-CH_2$) ppm; ESI MS: m/z = 295.1 [M-2I$^-$]$^{2+}$. Anal. Calcd for $C_{32}H_{32}I_2N_6NiO_2.H_2O$ (863.15): C 44.53, H 3.97, N 9.74. Found: C 44.71, H 3.87, N 9.61%. λ (nm)/ε ($M^{-1}{\cdot}cm^{-1}$), HEPES-buffered saline (pH 7.4): 370 (24550).

Complex **3**. This preparation closely followed the synthesis of complex **1**, starting from **IIc** (100 mg, 0.27 mmol) in MeOH (4 mL), $Ni(OAc)_2{\cdot}4H_2O$ (34 mg, 0.135 mmol) in MeOH (2 mL), *o*-phenylenediamine (15 mg, 0.135 mmol) in MeOH (2 mL), and triethylamine (40 μL, 0.29 mmol) were added. A red hygroscopic solid was obtained. Yield: 58%. ^{1}H NMR (400 MHz, [D_6]DMSO): δ = 9.11 (s, 2H, -N=CH); 8.82 (s, 2H, -N=CH-N); 8.13−8.11 (m, 2H, Ar−H); 7.79 (s, 2H, imid-H); 7.71 (s, 2H, imid-H); 7.39−7.34 (m, 4H, Ar−H); 7.21 (dd, J = 2 Hz, J = 8.8 Hz, 2H, Ar−H); 6.85 (d, J = 8.8 Hz, 2H, Ar−H); 4.22−4.19 (m, 4H, $-CH_2$); 3.85 (s, 6H, N$-CH_3$); 2.12−2.09 (m, 4H, $-CH_2$) ppm; ESI MS: m/z = 309.2 [M-2I$^-$]$^{2+}$. Anal. Calcd for $C_{34}H_{36}I_2N_6NiO_2.H_2O$ (891.21): C 45.82, H 4.30, N 9.43. Found: C 45.50, H 4.41, N 9.46%. λ (nm)/ε ($M^{-1}{\cdot}cm^{-1}$), HEPES-buffered saline (pH 7.4): 370 (26750).

Complex **4**. This preparation closely followed the synthesis of complex **1**, starting from 3-(3-formyl-4-hydroxybenzyl)-1-methyl-1*H*-imidazol-3-ium chloride (100 mg, 0.4 mmol) in MeOH (4 mL), $Ni(OAc)_2{\cdot}4H_2O$ (50 mg, 0.2 mmol) in MeOH (2 mL), **IIIc** (57 mg, 0.2 mmol) in MeOH (2 mL), and triethylamine (60 μL, 0.43 mmol) were added. A brown hygroscopic solid was obtained. Yield: 68%. ^{1}H NMR (400 MHz, [D_6]DMSO): δ = 9.58 (s, 1H, -N=CH-N); 9.28 (d, J = 10 Hz, 2H, -N=CH); 8.56 (s, 1H, -N=CH-N); 8.21 (d, J = 8.8 Hz, 1H, imid-H); 7.94 (s, 2H, -N=CH-N); 7.77 (s, 4H, Ar−H); 7.73 (s, 5H, Ar−H); 7.47 (d, J = 8.8 Hz, 1H, imid-H); 7.41 (d, J = 8.8 Hz, 2H, imid-H); 6.91 (d, J = 8.8 Hz, 2H, imid-H); 5.48 (s, 2H, −CH2); 5.34 (d, J = 4.2 Hz, 4H, $-CH_2$); 3.88 (s, 6H, N$-CH_3$); 3.86 (s, 3H, N$-CH_3$) ppm; ESI MS: m/z = 773.1 [M-Cl$^-$]$^+$, 729.2 [M-Br$^-$]$^+$. Anal. Calcd for $C_{35}H_{35}BrCl_2N_8NiO_2.8H_2O$ (953.33): C 44.09, H 5.39, N 11.75. Found: C 44.01, H 6.17, N 11.6%. λ (nm)/ε ($M^{-1}{\cdot}cm^{-1}$), HEPES-buffered saline (pH 7.4): 370 (15 560).

Complex **5**. This preparation closely followed the synthesis of complex **1**, starting from **Ic** (100 mg, 0.28 mmol) in MeOH (4 mL), $Ni(OAc)_2{\cdot}H_2O$ (35 mg, 0.14 mmol) in MeOH (2 mL), **IIIc** (40 mg, 0.14 mmol) in MeOH (2 mL), and triethylamine (43 μL, 0.31 mmol) were added. A red hygroscopic solid was obtained. Yield: 65%. ^{1}H NMR (400 MHz, [D_6]DMSO): δ = 9.24 (s, 1H, -N=CH-N); 9.05 (d, J = 7.2 Hz, 2H, -N=CH); 8.89 (d, J = 7.2 Hz, 2H, -N=CH-N); 8.31 (s, 1H, imid-H); 8.17 (d, J = 8.8 Hz, 1H, imid-H); 7.83 (s, 1H, Ar−H); 7.74 (d, J = 7 Hz, 3H, Ar−H); 7.69 (s, 2H, Ar−H); 7.41 (s, 1H, Ar−H); 7.39 (s, 2H, Ar−H); 7.25−7.21 (m, 2H, imid-H); 6.87 (dd, J = 4 Hz, J = 8.8 Hz, 2H, imid-H); 5.46 (s, 2H, $-CH_2$); 4.40 (dd, J = 6.9 Hz, J = 12.6 Hz, 4H, $-CH_2$); 3.88 (s, 3H, N$-CH_3$); 3.83 (d, J = 3.6 Hz, 6H, N$-CH_3$)); 3.05 (dd, J = 6.9 Hz, J = 12.6 Hz, 4H, $-CH_2$) ppm; ESI MS: m/z = 939.0 [M-Br$^-$]$^+$, 893.0 [M-I$^-$]$^+$. Anal. Calcd for $C_{37}H_{39}BrI_2N_8NiO_2.6H_2O$ (1128.26): C 39.39, H 4.55, N 9.93. Found: C 39.52, H 4.46, N 10.20%. λ (nm)/ε ($M^{-1}{\cdot}cm^{-1}$), HEPES-buffered saline (pH 7.4): 370 (18800).

Complex **6**. This preparation closely followed the synthesis of complex **1**, starting from **IIc** (100 mg, 0.27 mmol) in MeOH (4 mL), $Ni(OAc)_2{\cdot}4H_2O$ (34 mg, 0.135 mmol) in MeOH (2 mL), **IIIc** (38 mg, 0.135 mmol) in MeOH (2 mL), and triethylamine (40 μL, 0.29 mmol) were added. A brown hygroscopic solid was obtained. Yield: 53%. ^{1}H NMR (400 MHz, [D_6]DMSO): δ = 9.38 (s, 1H, -N=CH-N); 9.24 (s, 1H, -N=CH); 9.18 (s, 1H, -N=CH); 9.00 (s, 1H, -N=CH-N); 8.91 (s, 1H, -N=CH-N); 8.46 (s, 1H, imid-H); 8.20 (d, J = 8.8 Hz, 1H, imid-H); 7.89 (s, 1H, Ar−H); 7.82 (d, J = 8.8 Hz,2H, Ar−H); 7.74−7.70 (m, 3H, Ar−H); 7.49 (s, 1H, Ar−H); 7.44 (s, 2H, Ar−H); 7.24 (d, J = 8.8 Hz, 2H, imid-H); 6.87 (dd, J = 2.9 Hz, J = 8.8 Hz, 2H, imid-H); 5.47 (s, 2H, $-CH_2$); 4.24−4.20 (m, 4H, $-CH_2$); 3.89 (s, 6H, N$-CH_3$); 3.86 (s, 3H, N$-CH_3$); 2.97 (broad, 4H, $-CH_2$); 2.13−2.09 (m, 4H, $-CH_2$) ppm; ESI MS: m/z = 967.0 [M-Br$^-$]$^+$, 921.0 [M-I$^-$]$^+$. Anal. Calcd for $C_{39}H_{43}BrI_2N_8NiO_2.4H_2O$ (1120.28): C 41.81, H 4.59, N 10.00. Found: C 41.77, H 4.83, N 9.94%. λ (nm)/ε ($M^{-1}{\cdot}cm^{-1}$), HEPES-buffered saline (pH 7.4): 375 (17000).

Complex **7**. This preparation closely followed the synthesis of complex **1**, starting from **IIc** (100 mg, 0.27 mmol) in EtOH (4 mL), $Ni(OAc)_2{\cdot}4H_2O$ (34 mg, 0.135 mmol) in EtOH (2 mL), **IVf** (40 mg, 0.135 mmol) in EtOH (2 mL), and triethylamine (40 μL, 0.29 mmol) were added. A red hygroscopic solid was obtained. Yield: 78%. ^{1}H NMR (400 MHz, [D_6]DMSO): δ = 9.25 (s, 1H, -N=CH-N); 9.19 (s, 2H, -N=CH); 8.98 (s, 1H, -N=CH-N); 8.83 (s, 1H, -N=CH-N); 8.27 (s, 1H, imid-H); 8.07 (d, J = 8.8 Hz, 1H,imid-H); 7.84 (s, 1H, Ar−H); 7.81 (s, 1H, Ar−H); 7.76 (s, 1H, Ar−H); 7.72 (s, 2H, Ar−H); 7.68 (s, 1H, Ar−H); 7.52 (s, 1H, imid-H); 7.42 (s, 1H, imid-H); 7.24−7.17 (m, 3H, Ar−H); 6.85 (dd, J = 4.2 Hz, J = 8.8 Hz, 2H, imid-H); 4.64−4.60 (m, 2H, $-CH_2$); 4.24−4.20 (m, 4H, $-CH_2$); 3.87 (d, J = 6.6 Hz, 6H, N$-CH_3$); 3.84 (s, 3H, N$-CH_3$); 3.24 (broad, 2H, $-CH_2$); 2.92−2.91 (m, 4H, $-CH_2$); 2.15−2.09 (m, 4H, $-CH_2$) ppm; ESI MS: m/z = 981.1 [M-Br$^-$]$^+$, 935.1 [M-I$^-$]$^+$. Anal. Calcd for $C_{40}H_{45}BrI_2N_8NiO_2.6H_2O$ (1170.34): C 41.05, H 4.91, N 9.57. Found: C 40.99, H 5.25, N 9.02%. λ (nm)/ε ($M^{-1}{\cdot}cm^{-1}$), HEPES-buffered saline (pH 7.4): 375 (14 400).

Complex **8**. This preparation closely followed the synthesis of complex **1**, starting from 3-(3-formyl-4-hydroxybenzyl)-1-methyl-1*H*-imidazol-3-ium chloride (100 mg, 0.4 mmol) in MeOH (4 mL), $Ni(OAc)_2.4H_2O$ (50 mg, 0.2 mmol) in MeOH (2 mL), **IVf** (59 mg, 0.2 mmol) in MeOH (2 mL), and triethylamine (60 μL, 0.43 mmol) were added. A brown hygroscopic solid was obtained. Yield: 68%. ^{1}H NMR (400 MHz, [D_6]DMSO): δ = 9.39 (s, 1H, -N=CH-N); 9.31 (s, 2H, -N=CH); 9.26 (s, 1H, -N=CH-N); 9.18 (s, 1H, -N=CH-N); 8.32 (s, 1H, Ar−H); 8.08 (d, J = 8 Hz, 1H, imid-H); 7.79−7.74 (m, 6H, Ar−H); 7.69 (s, 2H, Ar−H); 7.39 (s, 2H, imid-H); 7.21 (d, J = 8 Hz, 1H, imid-H); 6.92 (d, J = 8 Hz, 2H, imid-H); 5.35 (d, J = 10 Hz, 4H, $-CH_2$); 4.65−4.62 (m, 2H, $-CH_2$); 4.04−4.03 (m, 2H, $-CH_2$); 3.88 (d, J = 10 Hz, 6H, N$-CH_3$); 3.84 (s, 3H, N$-CH_3$) ppm; ESI MS: m/z = 743.2 [M-Br$^-$]$^+$. Anal. Calcd for $C_{36}H_{37}BrCl_2N_8NiO_2.8H_2O$ (967.36): C 44.70, H 5.52, N 11.58. Found: C 44.57, H 5.81, N 11.31%. λ (nm)/ε ($M^{-1}{\cdot}cm^{-1}$), HEPES-buffered saline (pH 7.4): 367 (19750).

Complex **9**. This preparation closely followed the synthesis of complex **1**, salicylaldehyde (100 mg, 0.82 mmol) in MeOH (4 mL), $Ni(OAc)_2.4H_2O$ (102 mg, 0.41 mmol) in MeOH (2 mL), **IIIc** (123 mg, 0.41 mmol) in MeOH (2 mL), and triethylamine (126 μL, 0.90 mmol) were added. A brown hygroscopic solid was obtained. Yield:

dx.doi.org/10.1021/ic502063r | *Inorg. Chem.* 2014, 53, 12519−12531

Scheme 3. Synthetic Route for the Preparation of the Salicylaldehydes Precursors

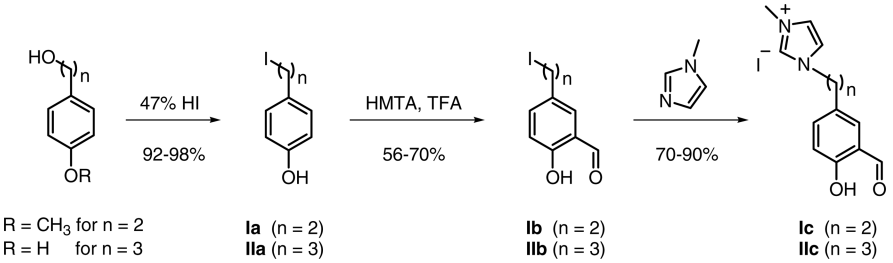

Scheme 4. Synthetic Routes for the Preparation of the Diamine Precursors

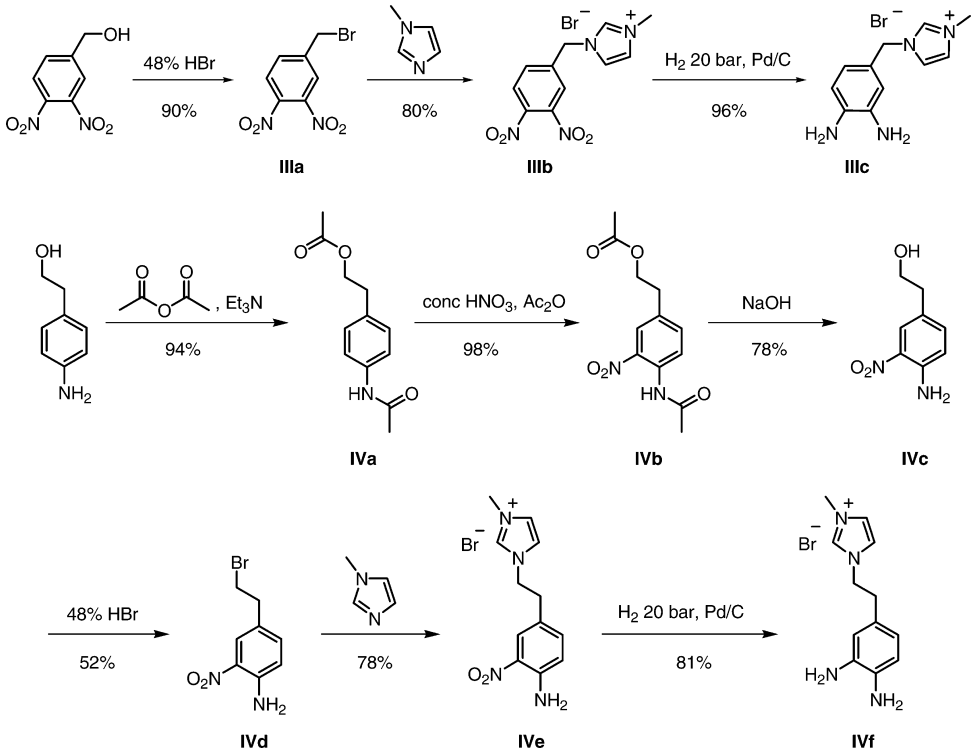

74%. ^{1}H NMR (400 MHz, [D$_6$]DMSO): δ = 9.28 (s, 1H, -N=CH-N); 8.91 (d, J = 7 Hz, 2H, -N=CH); 8.33 (s, 1H, Ar−H); 8.16 (d, J = 8 Hz, 1H, Ar−H); 7.86 (s, 1H, Ar−H); 7.75 (s, 1H, Ar−H); 7.61−7.56 (m, 2H, Ar−H); 7.38−7.32 (m, 3H, Ar−H); 6.86 (d, J = 8.5 Hz, 2H, Ar−H); 76.68 (s, 2H, imid-H); 5.44 (s, 2H, −CH$_2$); 3.87 (s, 3H, N−CH$_3$) ppm; ESI MS: m/z = 467.1 [M-Br$^-$]$^+$. Anal. Calcd for $C_{25}H_{21}BrN_4NiO_2.5H_2O$ (638.14): C 47.05, H 4.90, N 8.78. Found: C 47.06, H 5.62, N 8.35%. λ (nm)/ε ($M^{-1}\cdot cm^{-1}$), HEPES-buffered saline (pH 7.4): 370 (12200).

3. RESULTS AND DISCUSSION

3.1. Synthesis and Characterization of the Complexes.

Complexes **1**−**3** were synthesized by the condensation of 2 equiv of the appropriate 3-(3-formyl-4-hydroxy-phenalkyl)-1-methyl-3*H*-imidazol-1-ium salt with 1 equiv of 1,2-diamino-benzene and 1 equiv of Ni(OAc)$_2$·4H$_2$O under basic conditions. Complexes **4**−**8** were synthesized in a similar fashion using either 3-(3,4-diamino-benzyl)-1-methyl-3*H*-imidazol-1-ium bromide or 3-(3,4-diamino-phenethyl)-1-methyl-3*H*-imidazol-1-ium bromide instead of the 1,2-diaminobenzene. The archetype **9** was synthesized using salicylaldehyde instead of 3-(3-formyl-4-hydroxy-phenalkyl)-1-methyl-3*H*-imidazol-1-ium salt. The compounds were isolated as hygroscopic dark solids with yields ranging from 42 to 75%.

The general procedure for the synthesis of the starting aldehydes **Ic** and **IIc** is depicted in Scheme 3; the 3-(3-formyl-4-hydroxy-benzyl)-1-methyl-3*H*-imidazol-1-ium chloride was prepared according to a published procedure.[41] First, (4-methoxy-phenyl)-ethanol and 4-(2-hydroxyethyl)phenol were converted to 4-(2-iodoalkyl)phenol (**Ia** and **IIa**, respectively) by treatment with hydriodic acid under refluxing conditions. Next, 5-(2-iodoalkyl)salicylaldehydes **Ib** and **IIb** were formed via the use of HMTA in TFA. Finally, the precursors aldehyde were prepared through the quaternization reaction of *N*-methylimidazole to afford the imidazolium iodide salts (**Ic** and **IIc**).

The 3-(3,4-diamino-benzyl)-1-methyl-3*H*-imidazol-1-ium bromide (**IIIc**) spacer was synthesized from 4-(hydroxymethyl)-1,2-dinitrobenzene in a three-step synthetic procedure (Scheme 4). The first step was a bromination with 48% aqueous HBr, followed by nucleophilic substitution with the *N*-methylimidazole. The dinitroimidazolium salt was then reduced by H$_2$ (20 bar) in the presence of Pd/C catalyst to give the desired product **IIIc** in 69% overall yield. Preparation of 3-(3,4-diamino-phenethyl)-1-methyl-3*H*-imidazol-1-ium bromide (**IVf**) was achieved in six steps: 2-(4-aminophenyl)ethanol was treated with acetic anhydride and then nitric acid to give

dx.doi.org/10.1021/ic502063r | *Inorg. Chem.* 2014, 53, 12519−12531

the nitroacetamide **IVb**. Base hydrolysis afforded the unprotected 2-(4-amino-3-nitrophenyl)ethanol **IVc**. Treatment with 48% aqueous HBr and *N*-methylimidazole gave the corresponding imidazolium bromide, which was reduced by hydrogenation to produce the synthon **IVf**.

The ^{1}H NMR spectra of **1**−**9** are consistent with a low-spin electronic configuration of the nickel(II) ion; all ^{1}H resonances are observed in the diamagnetic window. In agreement with NMR data, the UV−vis spectra of the complexes display a charge transfer (CT) transition at ca. 370 nm, which is typical for square planar Ni(II)-salicylidene complexes.

Archetype **9** was isolated as single crystals by slow evaporation of methanol at room temperature. Its crystal structure is depicted in Figure 1. The nickel(II) ion resides

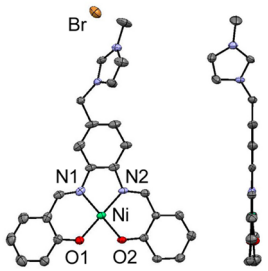

Figure 1. X-ray crystal structure of **9** shown with 30% thermal ellipsoids in top and side views. Hydrogen atoms were omitted for clarity.

within an essentially square planar geometry, coordinated by two phenolato oxygens (O1, O2) and two imino nitrogens (N1, N2). The coordination bond distances are as follows: Ni−O1, 1.844(3); Ni−O2, 1.840(4); Ni−N1, 1.856(4); and Ni−N2, 1.868(4) Å. These lengths are typical for a low-spin configuration of the nickel ion, and thus fully consistent with NMR spectroscopy data. The extent of distortion toward tetrahedral was estimated based on the dihedral angle between the O1−Ni−N1 and O2−Ni−N2 planes. The very small value of 3° indicates that almost no distortion is present. In addition, the angle between the phenolate rings is 7°, indicating that the overall geometry of the complex is preorganized for stacking over G-tetrads.

3.2. Analysis of DNA Interactions with Salophen Complexes. Different biophysical techniques have been developed for investigating G-quadruplex DNA/ligand interactions.[42] In the present study two different methods were employed, namely, FRET assays and SPR. Major advantages of the former technique are that several oligonucleotide sequences can be evaluated and that experiments can be automated using a multiwell plate reader. However, this technique is not the most appropriate for direct measurements of affinity constants. For this reason we also performed an SPR analysis, which allowed us to determine the thermodynamic parameters for the interaction.

3.2.1. FRET-Based Analysis of Affinity. The binding of the Ni(II)-salophen complexes **1**−**9** to G-quadruplexes was first investigated using FRET-based melting assays. The melting of the F21T human DNA telomere oligonucleotide in the presence of K^+ was monitored in the presence and absence of complexes. Each of the complexes evaluated stabilized the G-quadruplex structure (i.e., increased the G-quadruplex melting temperature) as shown in Figure 2 and Supporting Information, Figure S1. Stabilization is expressed as the

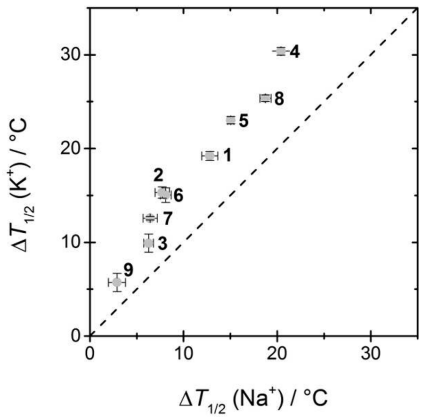

Figure 2. Thermal stabilization ($\Delta T_{1/2}$) induced by compounds **1**−**9** of the G-quadruplex structure formed by F21T in buffer containing 10 mM K^+ and 90 mM Li^+ ("K^+" conditions, *Y*-axis) vs $\Delta T_{1/2}$ in buffer with 100 mM Na^+ (*X*-axis).

difference in melting temperature ($\Delta T_{1/2}$). The extent of stabilization is high, as reflected by the concentration of the compounds in this experiment (0.5 μM), which is half the ligand concentration typically used in FRET melting assays.[27b,d,e,43] In the presence of higher concentrations of complex (1 μM is the typical concentration used in FRET melting assays) only partial melting of the G-quadruplex occurred, making accurate measurements of $\Delta T_{1/2}$ difficult.

The effect of the salophen substituents was evaluated by comparing the $\Delta T_{1/2}$ values. Compounds **1**−**3** contain the same unsubstituted diaminobenzene ring but differ in the lengths of the alkyl-imidazolium arms located para to the phenol moieties. The ligand-induced stabilization of the G-quadruplexes followed the trend: $\Delta T_{1/2}$ (**1**) > $\Delta T_{1/2}$ (**2**) > $\Delta T_{1/2}$ (**3**). Thus, shorter arms resulted in higher stabilization. The same conclusion was reached based on analysis of compounds **4**−**6**, which each bear a third imidazolium moiety on the diaminobenzene ring and differ in arm length ($\Delta T_{1/2}$ (**4**) > $\Delta T_{1/2}$ (**5**) > $\Delta T_{1/2}$ (**6**)). Further, comparison of melting of **7** (with a linker of three carbons) and **8** (with a linker of one) showed that the latter better stabilized the F21T sequence, and therefore that n' (the length of the third alkyl-imidazolium arm) is also a determinant in the binding strength. From these global comparisons, we conclude that alkyl-imidazolium arms with a single carbon linker in para position of the phenol moieties induce the highest stabilization of the F21T sequence for each of the tested substituents on the diaminobenzene ring.

The influence of the diaminobenzene substitution was also evaluated. The trends in thermal stabilization are $\Delta T_{1/2}$ (**4**) > $\Delta T_{1/2}$ (**8**) > $\Delta T_{1/2}$ (**1**); $\Delta T_{1/2}$ (**5**) > $\Delta T_{1/2}$ (**2**); and $\Delta T_{1/2}$ (**6**) > $\Delta T_{1/2}$ (**7**) > $\Delta T_{1/2}$ (**3**). In all three cases, the diaminobenzene functionalization increased the thermal stabilization. However, this functionalization alone induced only a weak G-quadruplex stabilization, as reflected by the small $\Delta T_{1/2}$ value measured for compound **9**.

The human telomeric sequence is known to adopt different conformations in Na^+- and K^+-containing solutions. The compound-induced stabilization was therefore also investigated in the presence of Na^+ (Figure 2 and Supporting Information, Figure S1). The influence of the substituents on the thermal stabilization was roughly similar in Na^+- as in K^+-containing medium. The $\Delta T_{1/2}$ values in the Na^+ medium were lower than

dx.doi.org/10.1021/ic502063r | *Inorg. Chem.* 2014, 53, 12519−12531

they were in the K^+-containing buffer for each complex evaluated. This behavior suggests that the compound-induced stabilization of the G-quadruplex also depends on its topology.[44]

To obtain insight into the structural dependence of the ligand binding, the $\Delta T_{1/2}$ values were determined for a set of sequences including one duplex and seven G-quadruplexes (Supporting Information, Table S1). The G-quadruplex sequences were chosen because they are representative of the structural diversity of G-quadruplexes. Figure 3 illustrates the

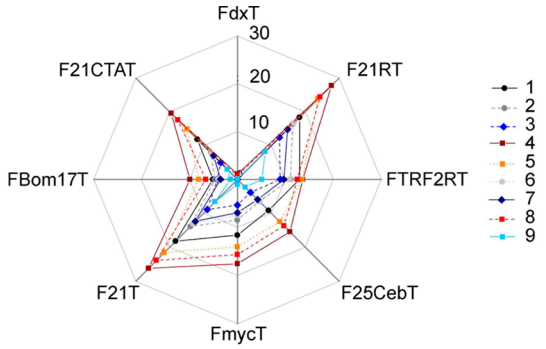

Figure 3. Structural selectivity profile. The thermal stabilization of the structures (in °C, from 0 to +30 °C) induced by compounds **1**–**9** is represented for structures adopted by eight oligonucleotide sequences. For clarity the error bars are reported only on Supporting Information, Figure S2. Detailed information related to the folding of the sequences is provided in Supporting Information, Table S1.

thermal stabilization due to binding of the salophen complexes in the presence of K^+ (for a more traditional presentation of the same data including error bars, see Supporting Information, Figure S2). No clear selectivity for a type of G-quadruplex structure (parallel, antiparallel, or 3 + 1) was observed. However, differences in $\Delta T_{1/2}$ values indicate that the magnitude of the stabilization is structure-dependent. The higher affinity of compounds with shorter alkylimidazolium arms observed with F21T was validated by analysis of the six other G-quadruplexes, suggesting that this trend is general. For each salophen complex the stabilization of the duplex sequence (FdxT) was significantly lower than that of the studied G-quadruplexes, which reflects the selectivity of these compounds. This selectivity was further confirmed by FRET melting assays in the presence of a duplex competitor (Supporting Information, Figures S3 and S4).

3.2.2. Surface Plasmon Resonance Studies. The binding affinity of complexes **1**–**8** for G-quadruplexes and double-stranded DNA was investigated by SPR. We employed a recently reported method based on use of a Template Assembled Synthetic G-Quadruplex (TASQ) that allows precise control of G-quadruplex topography through assembly of constrained structures on a template.[37] The biomolecular system consists in an intermolecular-like G-quadruplex motif **A** (parallel G-quadruplex conformation), an intramolecular G-quadruplex **B** (antiparallel like G-quadruplex conformation), and a duplex DNA **C** (see the Experimental Section for the structures of **A**, **B**, and **C**). The binding constants are reported in Table 1, and the sensorgrams are depicted in Figure 4 and Supporting Information.

Each complex evaluated had K_D values in the 0.1–2 μM range for both inter- and intramolecular topologies **A** and **B**. These values fall within the range of those reported for related

Table 1. Dissociation Constants for the Interaction of Complexes 1–8 with G-Quadruplex and Duplex DNA Structures[a]

complexes	intermolecular G-quadruplex **A**	intramolecular G-quadruplex **B**	hairpin duplex **C**	G_4 BMI index[b]
1	304 ± 30	1190 ± 100	1830 ± 200	3.9
2	1590 ± 160	1360 ± 140	n. d.[c]	0.9
3	1450 ± 140	1990 ± 200	n. d.[c]	1.4
4	209 ± 20	515 ± 50	n. d.[c]	2.5
5	680 ± 70	701 ± 80	n. d.[c]	1.0
6	750 ± 80	898 ± 90	n. d.[c]	1.2
7	500 ± 50	564 ± 60	n. d.[c]	1.1
8	142 ± 15	372 ± 40	4130 ± 400	2.6

[a] K_D in nM. [b] G_4 BMI: G-quadruplex Binding Mode index.[37b] [c] *n. d.*: The constants were not determined because of a very low affinity for the target duplex DNA (K_D > 10 μM).

compounds interacting with the HTelo sequence.[27d] It is significant that (i) the compounds with the lowest (i.e., best) K_D values measured by SPR are those that most significantly stabilized G-quadruplexes against heat denaturation and (ii) each salophen derivative tested had a higher affinity for G-quadruplex DNA structures than for duplex DNA. The K_D values were higher than 10 μM for duplex DNA **C** bound to each complex with the exceptions of **1** and **8** (1.8 μM and 4.1 μM, respectively). The tightest K_D measured was 142 nM for G-quadruplex DNA in complex with **8**. The greatest G-quadruplex versus duplex selectivity, defined as the ratio of the K_D values, was 50 for compound **4**.

The effect of the salophen substituents was evaluated by comparing the K_D values of the series of compounds for a given DNA structure. Complexes with shorter alkyl-imidazolium side-chains had higher affinity for G-quadruplexes than those with longer chains. For compounds **1**–**3** the K_D values for the interaction with G-quadruplex **A** are 304, 1590, 1450 nM and those for the interaction with G-quadruplex **B** are 1190, 1360, 1990 nM. The same trend was observed for complexes **4**–**6**: Complex **4**, with the shortest side chains connected in para position of the phenol moieties, had the highest affinity for both G-quadruplexes **A** and **B** (K_D of 209 nM and 515 nM, respectively) of the three complexes.

As expected, the incorporation of a third alkylimidazolium side chain on the diaminobenzene ring (complexes **4**–**8**) increased the affinity. In the case of G-quadruplex **A**, the K_D values fall within the range of 209–750 nM for **4**–**6**, whereas they are in the 304–1590 nM for complexes **1**–**3**, which do not harbor a third anchor. The K_D values for G-quadruplex **B** range between 515 and 898 nM for **4**–**6** and 1190 and 1990 nM for **1**–**3**. The influence of the length of the third alkylimidazolium side chain on the diaminobenzene ring was evaluated by comparing the relative affinities of complexes **4** and **8** (short linker) with those of complexes **6** and **7** (long linker) for G-quadruplex DNA. The K_D values for **8** are smaller than those of **4**, and similarly those measured for **7** are smaller than those of **6**. Thus, when connected to the diaminobenzene ring a longer alkyl-imidazolium chain tends to increase the affinity of the complexes for G-quadruplexes, although this effect was rather small. Of note, the K_D values for G-quadruplex **A** are generally lower than those for G-quadruplex **B**, showing a certain degree of selectivity of the complexes for intermolecular-like structures.

A numerical parameter, the G-quadruplex Binding Mode Index (G_4-BMI), has been introduced to enable comparison of

dx.doi.org/10.1021/ic502063r | *Inorg. Chem.* 2014, 53, 12519–12531

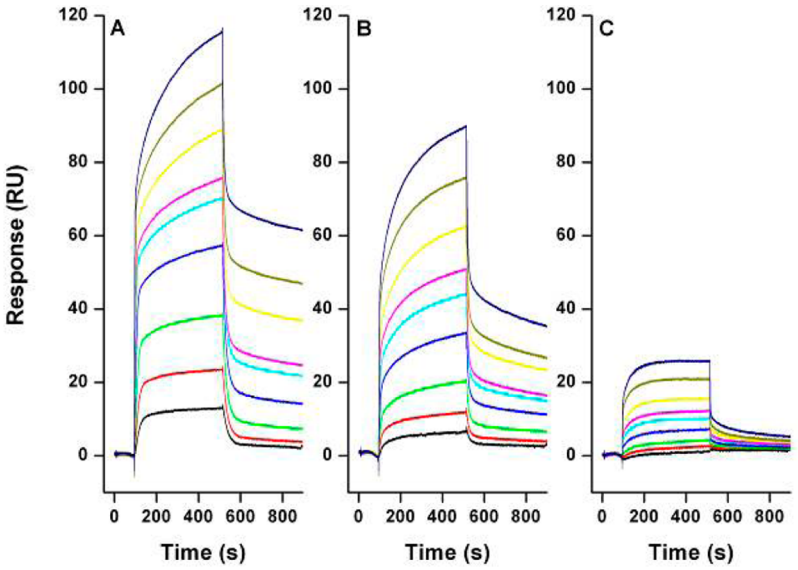

Figure 4. Sensorgrams of complex **8** in the presence of (A) an intermolecular parallel G-quadruplex **A**; (B) an intramolecular antiparallel G-quadruplex **B**; (C) a hairpin duplex DNA **C**. The complex concentrations were 25 nM (black), 50 nM (red), 100 nM (green), 200 nM (blue), 300 nM (cyan), 400 nM (magenta), 500 nM (yellow), 750 nM (dark yellow), 1 μM (navy blue).

the SPR-monitored binding mode of ligands.[37b] The G_4-BMI is defined as K_D-intra/K_D-inter, where K_D-intra is the K_D for intramolecular conformation **B**, and K_D-inter is the dissociation constant for intermolecular-like conformation **A**. The G_4-BMI values for the complexes tested are between 1 and 4. For compounds **1**, **4**, and **8** G_4-BMI values are very close to those reported for pentacyclic quinacridines harboring amino-containing side-chains, which are believed to interact with G-quadruplexes through mixed π-stacking over the guanine tetrad and electrostatic interactions in the grooves.[37b] Thus, the high flexibility of the cationic arms in the salophen series favors their positioning into the grooves, in addition to π-stacking over the quartet.

3.3. Computer Modeling Studies. To obtain further insights into the interactions between salophen derivatives and G-quadruplex DNA, molecular docking calculations were carried out. Complexes were docked to the human telomeric DNA structure (PDB entry 1KF1).[3c] To visualize the complex/quadruplex interactions, a noncovalent interaction (NCI) analysis was used.[35] This method calculates an index based on the electron density and the electron density gradient. This index presents singularities at low density when a weak interaction appears between two fragments. The isosurfaces of weak index values can be plotted to visualize the domains of noncovalent interactions. An arbitrary color code was chosen for NCI surfaces: red was assigned to regions associated with steric repulsions; blue was used for regions of strong attraction (for instance hydrogen bonding interactions); and green corresponds to regions with van der Waals (vdW) interactions.[35]

We focused our attention on the two features found to significantly influence the affinity of salophen complexes for G-quadruplexes: the number and the length of the side-chains on the salophen scaffold. As a starting point we considered complex **1**, with two short alkyl-imidazolium side-chains. Figure 5A shows the NCI surfaces observed when complex **1** and the G-quadruplex were docked. A good overlap is observed between the aromatic core of **1** and the guanines of the G-quadruplex. These stabilizing $\pi-\pi$ interactions are visualized on the plot as large green domains. The two side-chains are inserted into the opposite G-quadruplex grooves, and vdW interactions are observed between the imidazolium group and the nonbonding electron pair of guanine. Finally, a strong electrostatic interaction, highlighted by two black circles in Figure 5A, is established between the cationic side chains and one oxygen of the phosphate groups.

The NCI surface observed when complex **4**, bearing a third alkylimidazolium side chain, was docked with the G-quadruplex is similar to that obtained for **1**, with additional interactions due to the insertion of the third side chain into a third groove. The influence of the length of the side chains was evaluated by calculation of the NCI surface between complex **8** and the G-quadruplex (Figure 5C). The size of the region encompassing the vdW interactions between the imidazolium group and the nonbonding electron pair (indicated by black rectangles) was smaller for complex **8**, which has longer side-chains, than it was for complex **4**. This result likely explains the weaker affinity of **8** for G-quadruplex in comparison to **4**.

To quantify the strength of the interactions, density functional theory (DFT) calculations with the density functional method ωB97XD, which contains empirical dispersion terms and more correctly predicts noncovalent interactions than other methods, were performed. An estimation of the relative binding electronic energy was obtained using eq 1

$$\Delta E = (E_{M4} - E_4) - (E_{Mj} - E_j) \quad (1)$$

where E_{Mj} represents the electronic energy of the system formed by complex j and the first layer of the G-quadruplex, E_j is defined as the electronic energy of complex j. Complex **4** was taken as a reference in our calculation (E_{M4}). Within the investigated series, **4** was the agent with highest affinity for G-quadruplex (Table 2). By comparing the relative binding electronic energies of **4**, **5**, and **6** with **1**, **2**, and **3** the contribution of the third alkylimidazolium group in the binding energy was estimated to be more than 110 kcal/mol. By contrast, the influence of the length of the side chain was weaker, as demonstrated by the ΔE value for **3** that was only 23 kcal/mol higher than that for **1** and the ΔE value for **7** that was

dx.doi.org/10.1021/ic502063r | *Inorg. Chem.* 2014, 53, 12519−12531

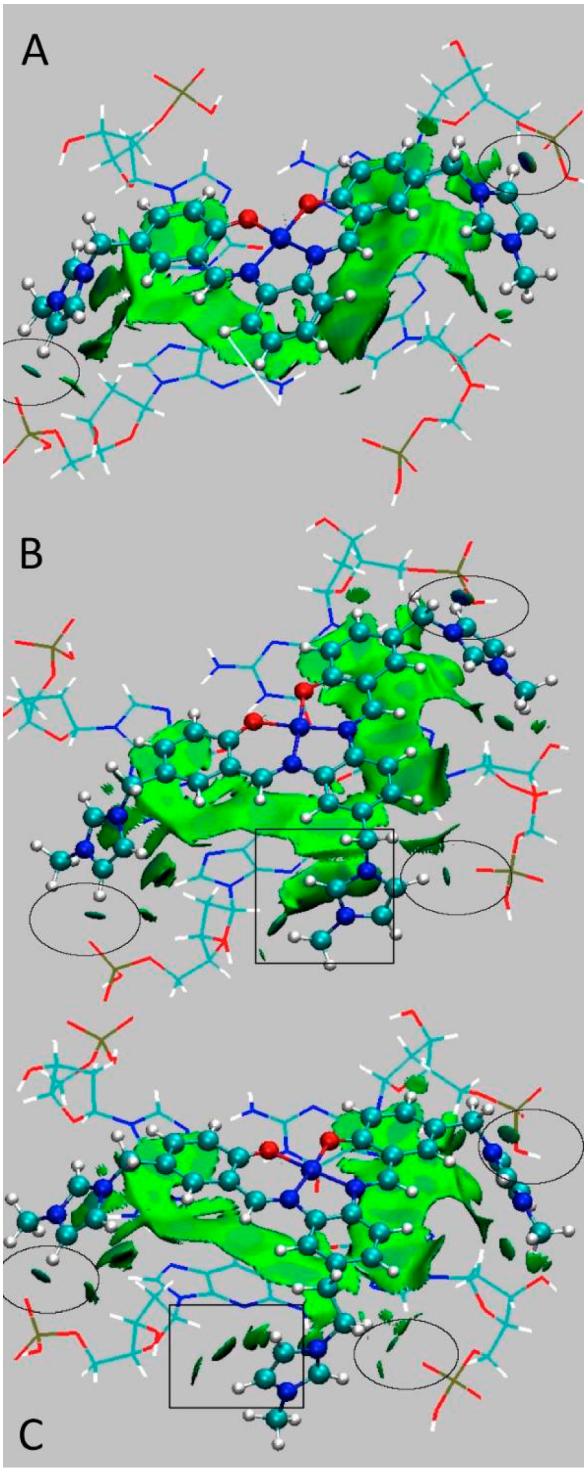

Figure 5. NCI surfaces and systems observed between the G-quadruplex and complexes (A) **1**, (B) **4**, and (C) **8**. The gradient cutoff is 0.5 au, and the color scale is $-0.07 < \rho < 0.07$ au.

21.3 kcal/mol higher than for **8**. The weak destabilization predicted for compounds having longer side-chains arises from a decrease in vdW interactions between the imidazolium groups and the nonbonding electron pair of guanine. An increase of the length of the side chains in compounds harboring a third arm modified the imidazolium orientation and disrupted vdW interactions with the guanines. The ΔE value calculated for **5** was 28.9 kcal/mol higher than that for **4**. Finally, it appears from this energetic analysis that differences in vdW interactions result in variations in affinity within the subseries **1**, **2**, and **3** and **4**, **5**, and **6**.

Table 2. Energy of Interaction of Complexes 1−8 with a G-Quadruplex Model Calculated by Using the ωB97XD/6-31g(d,p) Functional

complex	ΔE (eq 1)[a]
1	144.9
2	145.2
3	168
4	0
5	28.9
6	24.3
7	37.6
8	16.3

[a]Energies are given in kcal/mol, and values were normalized to that of complex **4**.

3.4. TRAP Assays. Biochemical evaluation of the complexes was performed by using a TRAP-G_4 assay that has been previously described to measure the ability of a compound to block telomerase-mediated extension of telomeric sequences.[39] In this assay, the inclusion of TS, TSG_4, and ITAS (an internal control that assesses nonspecific inhibition of Taq polymerase) allowed us to discriminate both between G_4-based and catalytic inhibition of telomerase as well as to evaluate the selectivity of compounds for G-quadruplexes compared to duplexes. The results of these experiments are summarized in Table 3 and Figure 6.

Table 3. TRAP G_4 Assays

complex	IC_{50} TRAP (μM)[a]	TRAP G_4 selectivity[a,b]
1	3 ± 0.35	6
2	2 ± 0.20	10
3	2 ± 0.25	10
4	1 ± 0.15	7
5	1 ± 0.08	7
6	0.7 ± 0.03	10
7	0.8 ± 0.03	7.5
8	0.7 ± 0.04	10

[a]Mean ± standard deviation of triplicates. [b]TRAP G_4 selectivity index corresponds to the ratio of IC_{50} ITAS to IC_{50} TRAP G_4

Global analysis of the biochemical data indicates that all the salophen complexes tested efficiently inhibited telomerase in vitro with IC_{50} ranging between 0.7 and 3 μM. The IC_{50} values of complexes **4**−**8** (0.7−1 μM) were lower than those of complexes **1**−**3** (2−3 μM). This result indicates that, as expected, the introduction of a third alkylimidazolium substituent on the diaminobenzene ring has a positive impact on the ability of salophen compounds to block telomerase activity. These assays suggest that the length of the side chains has only a minor effect on the inhibition of telomerase activity: the IC_{50} values measured for **1**, **2**, and **3** were 3, 2, and 2 μM, respectively, whereas those measured for **4**, **5**, and **6** were 1, 1, and 0.7 μM, respectively.

We further calculated the ratio of the IC_{50} of ITAS to the IC_{50} of TRAP-G_4, which reflects the selectivity of the compounds for telomerase inhibition. These ratios were between 6 and 10 for all the compounds, showing that these complexes were at least 6-fold more potent inhibitors of

dx.doi.org/10.1021/ic502063r | Inorg. Chem. 2014, 53, 12519−12531

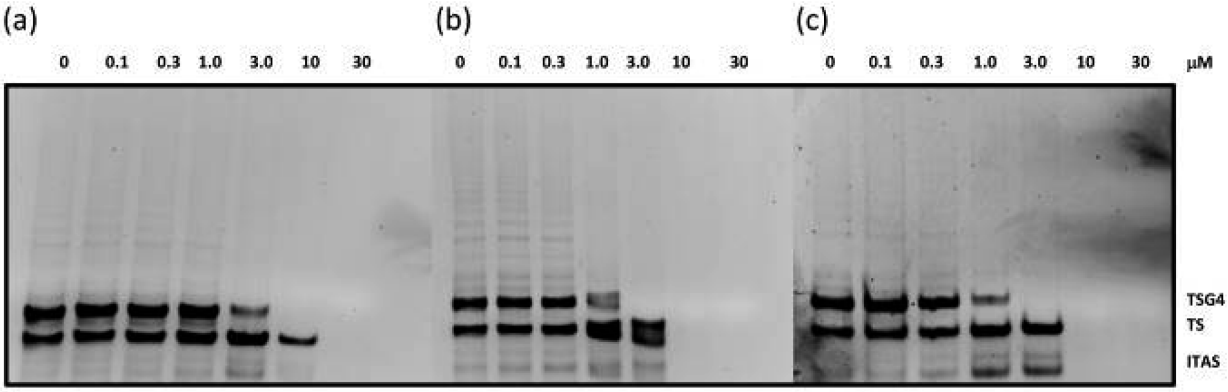

Figure 6. Inhibition of telomerase activity by complexes (A) **1**, (B) **4**, and (C) **8**. Increasing concentrations of complexes (0.1 to 30 μM) were added to 100 ng of telomerase extract in a TRAP G_4 assay. Positions of TS, TSG_4, and internal control ITAS PCR products are indicated. The IC_{50} value corresponds to the concentration required to inhibit 50% of the amplification of the TSG_4 fragment. In this assay, the inhibition of the catalytic activity of the telomerase is visualized as the inhibition of the TS signal, while the nonspecific interaction of molecules with duplex DNA or Taq polymerase is assessed by the loss of the ITAS signal.

telomerase activity than of Taq polymerase activity. Interestingly, salophen compounds bearing longer side chains (**3**, **6**, and **8**) were more selective inhibitors of telomerase than those with short arms. In addition, the selectivity of **1** (6-fold) for telomerase was similar to that of **4** (7-fold), whereas selectivities of **3** and **6** were identical (10-fold for both complexes). Thus, the enhanced inhibition of telomerase activity by salophen complexes bearing a third alkylimidazolium group did not alter the selectivity of these molecules toward duplex DNA.

4. CONCLUSION

Ni(II) complexes **1**−**9** were prepared based on salophen that contained different numbers (1, 2, or 3) of alkylimidazolium side chains that varied in the length from one carbon to three carbons. FRET-based thermal denaturation experiments demonstrated that each complex interacted strongly with the human telomeric sequence and stabilized the G-quadruplex structure. The extent of stabilization depended on the length of the side-chains of the ligands. The greatest stabilization of the F21T sequence was achieved with the shortest alkylimidazolium arms in the para position relative to the phenol moieties. Diaminobenzene functionalization, which was used to add a third anchor arm, alone induced a slight G-quadruplex stabilization. Compounds **1**−**8** were selective for G-quadruplexes versus duplex DNA. The structural selectivity for particular G-quadruplex isoforms was investigated by comparing the thermal stabilization of the F21T, FmycT, F25CebT, FBom17T, and F21CTAT sequences by the compounds. No clear discrimination for a particular folding type (parallel, antiparallel or 3 + 1) was observed, but the $\Delta T_{1/2}$ obtained with F21T in Na^+ medium in the presence of each of the complexes was lower than in K^+-containing buffer, suggesting that the binding strength is structure-dependent. The binding constants determined by SPR and stabilizations determined using FRET-based thermal melting analyses are in agreement. The K_D values for binding of complexes to G-quadruplexes were within the range from 142 to 1990 nM. None of the complexes bound tightly to duplex DNA; K_D values were higher than 10 μM for most of the complexes investigated. The shorter the side arms, the higher the affinity for G-quadruplexes. The introduction of a third anchor on the diaminobenzene bridge lowered the K_D values. The optimal G-quadruplex binders were **4** and **8**, with K_D values of 141 and 515 nM, respectively. The ratios of K_D values for parallel and antiparallel topologies were between 1 and 3.9 suggesting that the compounds interact both by π-stacking over the tetrad and electrostatic interactions in the grooves. Molecular modeling studies confirmed that the aromatic rings in **1** are involved in $\pi-\pi$ interactions with the guanines and that the side chains are inserted into opposite grooves. Stabilizing vdW interactions between the imidazolium groups and the nonbonding electrons pair of guanines were observed. Additional electrostatic interactions occur between one of the phosphate group oxygens and the side chains. Of note, the cationic side chains bind in opposite rather than adjacent grooves. This is in contrast to the binding mode of salophen complexes previously reported by Neidle et al.[27] This shows that discrimination between opposite versus adjacent groove insertion can be achieved by appropriate substitution (para vs meta) on the salophen backbone. As expected, the incorporation of a third alkylimidazolium side chain on the diaminobenzene ring (complexes **4**−**8**) results in additional interactions and improved the affinity. DFT calculations (ωB97XD functional) confirmed that the assemblies formed between the G-quadruplex and complexes with three side chains are significantly more stable than those formed with compounds having two side chains (ΔE of about 145 kcal/mol between **1** and **4**). The influence of side chain length is comparatively weaker (ΔE lower than 30 kcal/mol between **4** and **5**) and results from attenuation of the vdW interactions between the nonbonding electron pair of the G-quadruplex guanine and the imidazolium groups. Finally, all the compounds inhibit telomerase in vitro with IC_{50} values within the range of 0.7−3 μM. The most effective inhibitors were complexes **4**−**8** (0.7−1 μM), which contain the third alkylimidazolium anchor on the diaminobenzene ring.

■ ASSOCIATED CONTENT

Supporting Information

FRET melting oligonucleotides, comparative stabilization, FRET melting experiments with duplex competitor, SPR sensorgrams, TRAP assays, computer modeling studies, crystallographic structural data in CIF file. This material is available free of charge via the Internet at http://pubs.acs.org. CCDC-990056 contains the supplementary crystallographic data for this paper. These data can be obtained free of charge

from the Cambridge Crystallographic Data Centre via www.ccdc.cam.ac.uk/data_request/cif.

AUTHOR INFORMATION

Corresponding Author

*Fax: (+33) 476 51 4836. E-mail: Fabrice.Thomas@ujf-grenoble.fr.

Author Contributions

The manuscript was written through contributions of all authors. All authors have given approval to the final version of the manuscript.

Funding

This work was supported by ANR QUARPDIEMS (ANR-12-BSV8−0008−04), Labex ARCANE (ANR-11-LABX-0003−01), PRES Toulouse, Région Mydi-Pyrénées, and Région Aquitaine grants. The Nanobio-ICMG platform (FR 2603) is acknowledged for providing synthesis and purification of oligonucleotides and SPR facilities.

Notes

The authors declare no competing financial interest.

ACKNOWLEDGMENTS

The authors would like to sincerely acknowledge Prof. P. Labbé and Dr. J. Dejeu for their assistance in interpreting SPR data and for fruitful discussions.

REFERENCES

(1) (a) Todd, A. K.; Johnston, M.; Neidle, S. *Nucleic Acids Res.* **2005**, *33*, 2901−2907. (b) Huppert, J. L.; Balasubramanian, S. *Nucleic Acids Res.* **2005**, *33*, 2908−2916. (c) Tran, P. L. T.; Mergny, J. L.; Alberti, P. *Nucleic Acids Res.* **2011**, *39*, 3282−3291. (d) Mergny, J. L. *Nat. Chem. Biol.* **2012**, *8*, 225−226.

(2) (a) Sen, D.; Gilbert, W. *Nature* **1988**, *334*, 364−366. (b) Davies, J. T. *Angew. Chem., Int. Ed.* **2004**, *43*, 668−698. (c) Neidle, S. *Curr. Opin. Struct. Biol.* **2009**, *19*, 239−250. (d) Gonzalez-Rodriguez, D.; van Dongen, J. L. J.; Lutz, M.; Spek, A. L.; Schenning, A. P. H. J.; Meijer, E. W. *Nat. Chem.* **2009**, *1*, 151−155.

(3) (a) Smith, F. W.; Feigon, J. S. *Nature* **1992**, *356*, 164−168. (b) Wang, Y.; Patel, D. J. *Structure* **1993**, *1*, 263−282. (c) Parkinson, G. N.; Lee, M. P. H.; Neidle, S. *Nature* **2002**, *417*, 876−880. (d) Luu, K. N.; Phan, A. T.; Kuryavyi, V.; Lacroix, L.; Patel, D. J. *J. Am. Chem. Soc.* **2006**, *128*, 9963−9979. (e) Phan, A. T.; Kuryavyi, V.; Luu, K. N.; Patel, D. J. *Nucleic Acids Res.* **2007**, *35*, 6517−6725. (f) Lee, M. P. H.; Parkinson, G. N.; Hazel, P.; Neidle, S. *J. Am. Chem. Soc.* **2007**, *129*, 10106−10107.

(4) (a) Phan, A. T.; Patel, D. J. *J. Am. Chem. Soc.* **2003**, *125*, 15021−15027. (b) Burge, S.; Parkinson, G. N.; Hazel, P.; Todd, A. K.; Neidle, S. *Nucleic Acids Res.* **2006**, *34*, 5402−5415. (c) Hazel, P.; Parkinson, G. N.; Neidle, S. *Nucleic Acids Res.* **2006**, *34*, 2117−2127. (d) Dai, J.; Carver, M.; Yang, D. *Biochimie* **2008**, *90*, 1172−1183. (e) Lipps, H. J.; Rhodes, D. *Trends in Cell Biol.* **2009**, *19*, 414−422. (f) Viglasky, V.; Bauer, L.; Tluckova, K. *Biochemistry* **2010**, *49*, 2110−2120.

(5) (a) Blackburn, E. H. *Annu. Rev. Biochem.* **1984**, *53*, 163−194. (b) Wellinger, R. J.; Sen, D. *Eur. J. Cancer* **1997**, *33*, 735−749.

(6) (a) Blackburn, E. H. *Cell* **2001**, *106*, 661−673. (b) Blackburn, E. H. *Angew. Chem., Int. Ed.* **2010**, *49*, 7405−7421. (c) Rajpar, S.; Guittat, L.; Mergny, J. L. *Bull. Cancer* **2011**, *98*, 999−1009.

(7) (a) Todd, A. K. *Nucleic Acids Res.* **2007**, *35*, 5799−5808. (b) Huppert, J. L.; Balasubramanian, S. *Nucleic Acids Res.* **2007**, *35*, 406−413. (c) Yuan, L.; Tian, T.; Chen, Y.; Yan, S.; Xing, X.; Zhang, Z.; Zhai, Q.; Xu, L.; Wang, S.; Weng, X.; Yuan, B.; Feng, Y.; Zhou, X. *Sci. Rep.* **2013**, *3*, 1811.

(8) de Lange, T.; Shiue, L.; Myers, R. M.; Cox, D. R.; Naylor, S. L.; Killery, A. M.; Varmus, H. E. *Mol. Cell. Biol.* **1990**, *10*, 518−527.

(9) Kipling, D.; Cooke, H. J. *Nature* **1990**, *347*, 400−402.

(10) (a) Henderson, E. R.; Hardin, C. C.; Wolk, S. K.; Tinoco, I., Jr.; Blackburn, E. H. *Cell* **1987**, *51*, 899−908. (b) Henderson, E. R.; Blackburn, E. H. *Mol. Cell. Biol.* **1989**, *9*, 345−348.

(11) Greider, C. W. *Annu. Rev. Biochem.* **1996**, *65*, 337−365.

(12) Blackburn, E. H.; Gall, J. G. *J. Mol. Biol.* **1978**, *120*, 33−53.

(13) Klobutcher, L. A.; Swanton, M. T.; Donini, P.; Prescott, D. M. *Proc. Natl. Acad. Sci. USA* **1981**, *78*, 3015−3019.

(14) Okazaki, S.; Tsuchida, K.; Maekawa, H.; Ishikawa, H.; Fujiwara, H. *Mol. Cell. Biol.* **1993**, *13*, 1424−1432.

(15) O'Sullivan, R. J.; Karlseder, J. J. *Nat. Rev. Mol. Cell. Biol.* **2010**, *11*, 171−181.

(16) (a) Blackburn, E. H. *Nature* **1991**, *350*, 569−573. (b) Rhodes, D.; Giraldo, R. *Curr. Opin. Struct. Biol.* **1995**, *5*, 311−322.

(17) Olovnikov, A. M. *J. Theor. Biol.* **1973**, *41*, 181−190.

(18) (a) Palm, W.; de Lange, T. *Annu. Rev. Genet.* **2008**, *42*, 301−334. (b) de Lange, T. *Genes Dev.* **2005**, *19*, 2100−2110.

(19) Kim, N. W.; Piatyszek, M. A.; Prowse, K. R.; Harley, C. B.; West, M. D.; Ho, P. L.; Coviello, G. M.; Wright, W. E.; Weinrich, S. L.; Shay, J. W. *Science* **1994**, *266*, 2011−2015.

(20) Chan, S. R. W. L.; Blackburn, E. H. *Philos. Trans. R. Soc., B* **2004**, *359*, 109−121.

(21) Hahn, W. C.; Meyerson, M. *Ann. Med.* **2001**, *33*, 123−129.

(22) (a) Kerwin, S. M. *Curr. Pharm. Des.* **2000**, *6*, 441−478. (b) Han, H.; Hurley, L. H. *Trends Pharmacol. Sci.* **2000**, *21*, 136−142. (c) Neidle, S.; Read, M. A. *Biopolymers* **2001**, *56*, 195−208. (d) Balasubramanian, S.; Neidle, S. *Curr. Opin. Chem. Biol.* **2009**, *13*, 345−353. (e) Huppert, J. L. *Chem. Soc. Rev.* **2008**, *37*, 1375−1384. (f) Riou, J. F.; Morjani, H.; Trentesaux, C. *Ann. Pharm. Fr.* **2006**, *64*, 97−105. (g) Huppert, J. L. *Philos. Trans. R. Soc., A* **2007**, *365*, 2969−2984. (h) Oganesian, L.; Bryan, T. M. *BioEssays* **2007**, *29*, 155−165. (i) Ou, T. M.; Lu, Y. J.; Tan, J. H.; Huang, Z. S.; Wong, K. Y.; Gu, L. Q. *ChemMedChem* **2008**, *3*, 690−713. (j) De Cian, A.; Lacroix, L.; Douarre, C.; Temime-Smaali, N.; Trentesaux, C.; Riou, J. F.; Mergny, J. L. *Biochimie* **2008**, *90*, 131−155. (k) Yang, D.; Okamoto, K. *Future Med. Chem.* **2010**, *2*, 619−646.

(23) (a) Neidle, S.; Parkinson, G. N. *Biochimie* **2008**, *90*, 1184−1196. (b) Monchaud, D.; Teulade-Fichou, M. P. *Org. Biomol. Chem.* **2008**, *6*, 627−636. (c) Neidle, S. *Curr. Opin. Struct. Biol.* **2009**, *19*, 239−250. (d) Haider, S. M.; Neidle, S.; Parkinson, G. N. *Biochimie* **2011**, *93*, 1239−1251. (e) Chen, Y.; Yang, D. *Curr. Protoc. Nucleic Acid Chem.* **2012**, *50*, 17.5.1−17.5.17.

(24) Georgiades, S. N.; Karim, N. H. A.; Suntharalingam, K.; Vilar, R. *Angew. Chem., Int. Ed.* **2010**, *49*, 4020−4034.

(25) (a) Kim, M. Y.; Vankayalapati, H.; Shin-Ya, K.; Wierzba, K.; Hurley, L. H. *J. Am. Chem. Soc.* **2002**, *124*, 2098−2099. (b) Sun, D.; Thompson, B.; Cathers, B. E.; Salazar, M.; Kerwin, S. M.; Trent, J. O.; Jenkins, T. C.; Neidle, S.; Hurley, L. H. *J. Med. Chem.* **1997**, *40*, 2113−2116.

(26) (a) Wheelhouse, R. T.; Sun, D.; Han, H.; Xiaogang Han, F.; Hurley, L. H. *J. Am. Chem. Soc.* **1998**, *120*, 3261−3262. (b) Izbicka, E.; Wheelhouse, R. T.; Raymond, E.; Davidson, K. K.; Lawrence, R. A.; Sun, D.; Windle, B. E.; Hurley, L. H.; Von Hoff, D. D. *Cancer Res.* **1999**, *59*, 639−644. (c) Shi, D. F.; Wheelhouse, R. T.; Sun, D.; Hurley, L. H. *J. Med. Chem.* **2001**, *44*, 4509−4523. (d) Keating, L. R.; Szalai, V. A. *Biochemistry* **2004**, *43*, 15891. (e) Parkinson, G. N.; Ghosh, R.; Neidle, S. *Biochemistry* **2007**, *46*, 2390−2397. (f) Evans, S. E.; Mendez, M. A.; Turner, K. B.; Keating, L. R.; Grimes, R. T.; Melchoir, S.; Szalai, V. A. *J. Biol. Inorg. Chem.* **2007**, *12*, 1235−1249. (g) Romera, C.; Bombarde, O.; Bonnet, R.; Gomez, D.; Dumy, P.; Calsou, P.; Gwan, J. F.; Lin, J. H.; Defrancq, E.; Pratviel, G. *Biochimie* **2011**, *93*, 1310−1317. (h) Pan, J.; Zhang, S. *J. Biol. Inorg. Chem.* **2009**, *14*, 401−407. (i) Nicoludis, J. M.; Miller, S. T.; Jeffrey, P. D.; Barrett, S. P.; Rablen, P. R.; Lawton, T. J.; Yatsunyk, L. A. *J. Am. Chem. Soc.* **2012**, *134*, 20446−20456. (j) Xu, H. J.; Stefan, L.; Haudecoeur, R.; Vuong, S.; Richard, P.; Denat, F.; Barbe, J. M.; Gros, P. G.; Monchaud, D. *Org. Biomol. Chem.* **2012**, *10*, 5212−5218. (k) Pradines, V.; Pratviel, G. *Angew. Chem., Int. Ed.* **2013**, *52*, 2185−2188. (l) Inui, Y.; Fukuzumi, S.; Kojima, T. *Dalton Trans.* **2013**, *42*, 3779−3782.

(27) (a) Reed, J. E.; Arola-Arnal, A.; Neidle, S.; Vilar, R. *J. Am. Chem. Soc.* **2006**, *128*, 5992−5293. (b) Arola-Arnal, A.; Benet-Bucholz, J.; Neidle, S.; Vilar, R. *Inorg. Chem.* **2008**, *47*, 11910−11919. (c) Wu, P.; Ma, D. L.; Leung, C. H.; Yan, S. C.; Zhu, N.; Abagyan, R.; Che, C. M. *Chem.—Eur. J.* **2009**, *15*, 13008−13028. (d) Campbell, N. H.; Karim, N. H. A.; Parkinson, G. N.; Gunaratnam, M.; Petrucci, V.; Todd, A. K.; Vilar, R.; Neidle, S. *J. Med. Chem.* **2012**, *55*, 209−222. (e) Karim, N. H. A.; Mendoza, O.; Shivalingam, A.; Thompson, A. J.; Ghosh, S.; Kuimova, M. K.; Vilar, R. *RSC Adv.* **2014**, *4*, 3355−3363.

(28) Zahler, A. M.; Williamson, J. R.; Cech, T. R.; Prescott, D. M. *Nature* **1991**, *350*, 718−720.

(29) Salvati, E.; Leonetti, C.; Rizzo, A.; Scarsella, M.; Mottolese, M.; Galati, R.; Sperduti, I.; Stevens, M. F.; D'Incalci, M.; Blasco, M. *J. Clin. Invest.* **2007**, *117*, 3236−3247.

(30) (a) Gomez, D.; Wenner, T.; Brassert, B.; Douarre, C.; O'Donohue, M. F.; El Khoury, V.; Shin-ya, K.; Morjani, H.; Trentesaux, C.; Riou, J. F. *J. Biol. Chem.* **2006**, *281*, 38721−38729. (b) Phatak, P.; Cookson, J. C.; Dai, F.; Smith, V.; Gartenhaus, R. B.; Stevens, M. F. G.; Burger, A. M. *Br. J. Cancer* **2007**, *96*, 1223−1233. (c) Rodriguez, R.; Muller, S.; Yeoman, J. A.; Trentesaux, C.; Riou, J. F.; Balasubramanian, S. *J. Am. Chem. Soc.* **2008**, *130*, 15758−15759.

(31) Dolomanov, O. V.; Bourhis, L. J.; Gildea, R. J.; Howard, J. A. K.; Puschmann, H. *J. Appl. Crystallogr.* **2009**, *42*, 339−341.

(32) Frisch, M. J.; Trucks, G. W.; Schlegel, H. B.; Scuseria, G. E.; Robb, M. A.; Cheeseman, J. R.; Scalmani, G.; Barone, V.; Mennucci, B.; Petersson, G. A.; Nakatsuji, H.; Caricato, M.; Li, X.; Hratchian, H. P.; Izmaylov, A. F.; Bloino, J.; Zheng, G.; Sonnenberg, J. L.; Hada, M.; Ehara, M.; Toyota, K.; Fukuda, R.; Hasegawa, J.; Ishida, M.; Nakajima, T.; Honda, Y.; Kitao, O.; Nakai, H.; Vreven, T.; Montgomery, J. A., Jr.; Peralta, J. E.; Ogliaro, F.; Bearpark, M.; Heyd, J. J.; Brothers, E.; Kudin, K. N.; Staroverov, V. N.; Kobayashi, R.; Normand, J.; Raghavachari, K.; Rendell, A.; Burant, J. C.; Iyengar, S. S.; Tomasi, J.; Cossi, M.; Rega, N.; Millam, J. M.; Klene, M.; Knox, J. E.; Cross, J. B.; Bakken, V.; Adamo, C.; Jaramillo, J.; Gomperts, R.; Stratmann, R. E.; Yazyev, O.; Austin, A. J.; Cammi, R.; Pomelli, C.; Ochterski, J. W.; Martin, R. L.; Morokuma, K.; Zakrzewski, V. G.; Voth, G. A.; Salvador, P.; Dannenberg, J. J.; Dapprich, S.; Daniels, A. D.; Farkas, Ö.; Foresman, J. B.; Ortiz, J. V.; Cioslowski, J.; Fox, D. J. *Gaussian 09*, Revision D.01; Gaussian, Inc.: Wallingford, CT, 2009.

(33) Morris, G. M.; Goodsell, D. S.; Halliday, R. S.; Huey, R.; Hart, W. E.; Belew, R. K.; Olson, A. J. *J. Comput. Chem.* **1998**, *19*, 1639−1662.

(34) *SYBYL*, Tripos Associates: St Louis, MO.

(35) Contreras-García, J.; Johnson, E. R.; Keinan, S.; Chaudret, R.; Piquemal, J.-P.; Beratan, D. N.; Yang, W. *J. Chem. Theory Comput.* **2011**, *7*, 615−625.

(36) (a) De Cian, A.; Guittat, L.; Kaiser, M.; Saccà, B.; Amrane, S.; Bourdoncle, A.; Alberti, P.; Teulade-Fichou, M.-P.; Lacroix, L.; Mergny, J. L. *Methods* **2007**, *42*, 183−195. (b) Renčiuk, D.; Zhou, J.; Beaurepaire, L.; Guédin, A.; Bourdoncle, A.; Mergny, J. L. *Methods* **2012**, *57*, 122−128.

(37) (a) Murat, P.; Cressend, D.; Spinelli, N.; Van der Heyden, A.; Labbé, P.; Dumy, P.; Defrancq, E. *ChemBioChem* **2008**, *9*, 2588−2591. (b) Murat, P.; Bonnet, R.; Van der Heyden, A.; Spinelli, N.; Labbe, P.; Monchaud, D.; Teulade-Fichou, M. P.; Dumy, P.; Defrancq, E. *Chem.—Eur. J.* **2010**, *16*, 6106−6114.

(38) Obtained by retroviral transduction of the HT1080 cell line with the pbabe hTERT plasmid. See: Counter, C. M.; Hahn, W. C.; Wei, W.; Dickinson Caddle, S.; Beijersbergen, R. L.; Lansdorp, P. M.; Sedivy, J. M.; Weinberg, R. A. *Proc. Natl. Acad. Sci. U.S.A.* **1998**, *95*, 14723−14728.

(39) Gomez, D.; Mergny, J. L.; Riou, J. F. *Cancer Res.* **2002**, *62*, 3365−3368.

(40) Ji, C.; Peters, D. G. *J. Chem. Educ.* **2006**, *83*, 290−291.

(41) Naik, P. U.; McManus, G. J.; Zaworotko, M. J.; Singer, R. D. *Dalton Trans.* **2008**, 4834−4836.

(42) (a) Jaumot, J.; Gargallo, R. *Curr. Pharm. Des.* **2012**, *18*, 1900−1916. (b) Murat, P.; Singh, Y.; Defrancq, E. *Chem. Soc. Rev.* **2011**, *40*, 5293−5307.

(43) (a) Bertrand, B.; Stefan, L.; Pirrotta, M.; Monchaud, D.; Bodio, E.; Richard, P.; Le Gendre, P.; Warmerdam, E.; de Jager, M. H.; Groothuis, G. M. M.; Picquet, M.; Casini, A. *Inorg. Chem.* **2014**, *53*, 2296−2303. (b) Jäger, K.; Bats, J. W.; Ihmels, H.; Granzhan, A.; Uebach, S.; Patrick, B. O. *Chem.—Eur. J.* **2012**, *18*, 10903−10915. (c) Largy, E.; Hamon, F.; Rosu, F.; Gabelica, V.; De Pauw, E.; Guédin, A.; Mergny, J. L.; Teulade-Fichou, M. P. *Chem.—Eur. J.* **2011**, *17*, 13274−13283. (d) Long, Y.; Li, Z.; Tan, J. H.; Ou, T. M.; Li, D.; Gu, L. Q.; Huang, Z. S. *Bioconj. Chem.* **2012**, *23*, 1821−1831. (e) Petenzi, M.; Verga, D.; Largy, E.; Hamon, F.; Doria, F.; Teulade-Fichou, M.-P.; Guédin, A.; Mergny, J. L.; Mella, M.; Freccero, M. *Chem.—Eur. J.* **2012**, *18*, 14487−14496. (f) Smith, N. M.; Labrunie, G.; Corry, B.; Tran, P. L. T.; Norret, M.; Djavaheri-Mergny, M.; Raston, C. L.; Mergny, J. L. *Org. Biomol. Chem.* **2011**, *9*, 6154−6162. (g) Stefan, L.; Bertrand, B.; Richard, P.; Legendre, P.; Denat, F.; Picquet, M.; Monchaud, D. *ChemBioChem* **2012**, *13*, 1905−1912.

(44) Hamon, F.; Largy, E.; Guédin-Beaurepaire, A.; Rouchon-Dagois, M.; Sidibe, A.; Monchaud, D.; Mergny, J. L.; Riou, J. F.; Nguyen, C. H.; Teulade-Fichou, M. P. *Angew. Chem., Int. Ed.* **2011**, *50*, 8745−8749.